

COGNITIVE NEUROSCIENCE

Communication before coherence

Edmund T. Rolls,^{1,2} Tristan J. Webb³ and Gustavo Deco⁴¹Oxford Centre for Computational Neuroscience, Oxford, UK²Department of Computer Science, University of Warwick, Coventry CV4 7AL, UK³Department of Computer Science and Complexity Science Centre, University of Warwick, Coventry, UK⁴Theoretical and Computational Neuroscience, Universitat Pompeu Fabra, Barcelona, Spain

Keywords: communication through coherence, decision-making, information transmission, oscillations, synchrony

Abstract

The hypothesis of communication through coherence proposes that coherent or synchronous oscillations in connected neural systems can promote communication. It has been applied mainly to how oscillations interact in connected networks. We tested by simulations whether information transmission about an external stimulus from one network to a second network is influenced by gamma oscillations, by whether the oscillations are coherent, and by their phase. Gamma oscillations were induced by increasing the relative conductance of AMPA to NMDA excitatory synapses. It was found that small associative connection strengths between the networks were sufficient to produce information transmission (measured by Shannon mutual information) such that the second attractor network took the correct decision based on the state of the first network. Although gamma oscillations were present in both networks, the synaptic connections sufficient for perfect information transmission about the stimulus presented to the network (100% correct, 1 bit of information) were insufficiently strong to produce coherence, or phase-locking, between the two networks; this only occurred when the synaptic strengths between the networks were increased by $> 10 \times$. Further, the phase of the oscillations between the networks did not influence the information transmission or its speed at these connection strengths. Moreover, information transmission was as good when the AMPA-to-NMDA ratio was reduced to its normal value, and oscillations were not present. Similar results were found when the second network was not an attractor decision-making network. Thus information transmission can occur before synapses have been made sufficiently strong to produce coherence.

Introduction

Gamma-band synchronization has been found in many cortical areas and in a variety of tasks. It has been studied most extensively in the visual cortex of cats and monkeys (Gray *et al.*, 1989; Fries *et al.*, 2001, 2008; Womelsdorf *et al.*, 2006, 2007). Several authors have proposed that these synchronizations influence the interactions among neuronal groups (Salinas & Sejnowski, 2001; Varela *et al.*, 2001), a hypothesis referred to as communication through coherence (CTC; Fries, 2005, 2009).

Buehlmann & Deco (2010) set up a test of the hypothesis by modelling two interconnected integrate-and-fire neuronal networks. Both were attractor decision-making networks (Wang, 2002, 2008; Rolls & Deco, 2010). The first network could connect to the second by forward connections to the second, and, to model the situation in the cerebral neocortex, there were also backprojections, typically set to be one-third of the value of the forward connections. They were able to induce gamma oscillations in the range 50–70 Hz in both networks by increasing the conductance of the short time-constant (2 ms) AMPA receptor-activated channels relative to the long time-constant (100 ms) NMDA receptor-activated ion channels. They measured effects of one network on the other using transfer entropy (analogous to Granger

causality – Granger, 1969; Ding *et al.*, 2006; Ge *et al.*, 2012) which uses time differences between the networks to measure influence. They found effects with the transfer entropy measure, but this reflected the fact that oscillations in the networks were influencing each other, not information transmission about an external event or stimulus through the system.

Here, we performed a different experiment in which an external stimulus applied to one of two decision-making neuronal populations or pools of neurons could encourage the first network to take a decision, in which one decision pool reached a higher firing rate than the other population. We note that differences in firing rates between different neurons are part of the normal representation of information in cortical areas including the inferior temporal visual cortex, hippocampus, orbitofrontal cortex, anterior cingulate cortex and insular taste cortex (Rolls & Treves, 2011), so we are investigating a biologically realistic situation, to test whether in this situation coherence makes an important contribution to information transmission between coupled networks. We measured how the decisions taken by the second network depended on how strong the connections were from the first to the second network. In this way we were able to measure the information transmission, using Shannon information theory (Cover & Thomas, 1991; Rolls & Treves, 2011), to assess what information was transmitted from the first to the second network, and also the percentage correct performance of the second network. We measured how this depended on whether there were oscillations in both of the networks (by altering the g_{AMPA} to g_{NMDA} ratio), and we

Correspondence: Edmund T. Rolls, ¹Oxford Centre for Computational Neuroscience, as above. E-mail: edmund.rolls@oxcns.org

Received 16 December 2011, accepted 14 May 2012

were also able to measure whether the transmitted information depended on or was influenced by whether the networks were coherent, and were phase-locked into synchrony. We were able to do this not only by measuring the neuronal spiking but also by measuring the synaptically activated currents in the neurons, which provides a surrogate measure of the local field potentials which are believed to be generated by these currents (Mazzoni *et al.*, 2008). We also extended the findings to connected networks in which the second network was not an attractor decision-making network, but in which its firing rates reflected the state of the first network and thus of the stimulus that had been presented to the first network.

Materials and methods

The network used to investigate information transmission

The network model consists of two parts (Fig. 1). Network 1 (Net 1 or N1) is an attractor decision-making network that receives an external input λ_1 at time = 1000 ms that makes decision neuronal population 1 (decision pool 1; D1) win with a latency of ~ 500 ms. Pool N1D1 is connected to Network 2 (Net 2) decision pool 1 (N2D1) with forward synaptic connection strengths ω_f and backward synaptic connection strengths ω_b . ω_b was set to be 1/3 of the value of ω_f , as the forward connections are stronger in the brain (Rolls, 2008b; Section 1.11, pp 31–36), and because this ratio was found by Buehlmann & Deco (2010) to be effective in enhancing coherent oscillations. In a corresponding way pool N1D2 is connected to Network 2 decision pool 2 (N2D2) with forward and backward connection strengths that are the same as those for the D1 pools (see Fig. 1, and Table 2 for a complete specification of all the connections in the network; these correspond to those used by Buehlmann & Deco, 2010). Both Net 1 and Net 2 were set up to have gamma oscillations by increasing the g_{AMPA} to g_{NMDA} factor (defined below as δ) to a value of 0.1. (The short time constant of the AMPA receptors promotes oscillations, which are normally weak or absent at the normal ratio of NMDA to AMPA that we use as shown in Table 1 (Rolls & Deco, 2010; Buehlmann & Deco, 2010).)

To enable Net 1 to have gamma oscillations, we modelled it as an attractor decision-making network with the NMDA-to-AMPA conductance ratio reduced as described elsewhere. The architecture and operation of Net 1 were essentially similar to those of Net 2. Thus they oscillated in approximately the same way, and this enabled us to test, when they were oscillating and had the same generic architecture and underlying dynamics, whether coherence of the oscillations influenced the information transfer. With respect to Net 2, it was set up using a mean field analysis (Wang, 2002; Deco & Rolls, 2006; Rolls & Deco, 2010) so that it operated as an attractor network for almost all of the investigations reported. However, just to double check that the same generic results were obtained when Net 2 was not an attractor network, we reduced ω_+ in Net 2 for the experiment shown in Fig. 10.

The plan of the investigations was to increase the values of the connecting weights (ω_f and ω_b , and those that were scaled by these values as defined in section Implementation of the integrate-and-fire attractor neuronal network model of information transmission) between N1D1 and N2D1 from 0 upwards, to determine when N2D1 started to take the correct decision, and to examine how extensive measures of coherence, phase, and synchrony between the two networks were related to the amount of information transmitted, to the percentage correct of Net 2, and to the latency of the decision in Net 2. The communication through coherence (CTC) hypothesis holds that communication is facilitated by coherence (Fries, 2005, 2009). The communication between Net 1 and Net 2 was measured in the present investigations by the information transmitted between the networks, by the percentage correct of the second network, and by the latency of a correct response in Net 2. The advantage to testing this by simulation is that we have precise control over all the parameters that influence the operation of the system, and we can measure all the properties of the system. The aim was to show whether, in this well defined situation, information transmission was facilitated by coherence in the gamma frequency range. Indeed, to make the results relevant to understanding cortical function, the model we investigated is an integrate-and-fire model with spiking neurons and dynamically modelled synapses, as described in detail in other parts of Materials and methods and elsewhere (Rolls & Deco, 2010).

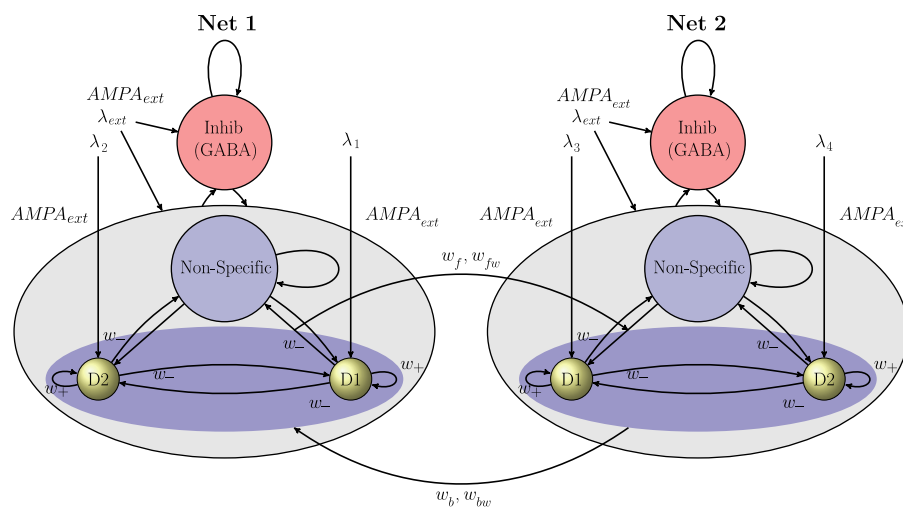


FIG. 1. Schematic representation of the network. The network consists of two connected attractor decision-making nets, Net 1 and Net 2. There are feedforward (ω_f) and feedback (ω_b) connections between Net 1 and Net 2. Inputs are applied to Net 1 λ_1 and λ_2 , which takes a decision with Net 1 decision pool 1 (N1D1) winning. Through the connections (ω_f) Net 2 pool D1 is encouraged to win the competition in Net 2. The network allows information transmission from Net 1 to influence the decision made by Net 2 to be investigated, to determine how it is influenced by the connection strength (ω_f) and whether there are oscillations in both Nets 1 and 2, which may or may not be coherent. There are external inputs (λ_{ext}) to simulate the spontaneous activity being received from other neurons in the system. Each decision pool has strong recurrent connection strengths (ω_+) to enable the pool to act as part of an attractor decision-making net. The strengths of the other synapses are shown, and are described in the text.

TABLE 1. The default parameter set used in the integrate-and-fire simulations

Global constants			
$V_L = -70$ mV $V_E = 0$ mV	$V_{thr} = -50$ mV $\alpha = 0.5$ /ms	$V_{reset} = -55$ mV	$V_1 = -70$ mV
Inhibitory neuron constants			
$C_m = 0.2$ nF $g_{AMPA,ext} = 1.62$ nS $\tau_{AMPA} = 2$ ms	$g_m = 20$ nS $g_{AMPA,rec} = 0.081$ nS $\tau_{NMDA,decay} = 100$ ms	$\tau_{rp} = 1$ ms $g_{NMDA} = 0.258$ nS $\tau_{NMDA,rise} = 2$ ms	$\tau_m = 10$ ms $g_{GABA} = 0.973$ nS $\tau_{GABA} = 10$ ms
Excitatory neuron constants			
$C_m = 0.5$ nF $g_{AMPA,ext} = 2.08$ nS $\tau_{AMPA} = 2$ ms	$g_m = 25$ nS $g_{AMPA,rec} = 0.104$ nS $\tau_{NMDA,decay} = 100$ ms	$\tau_{rp} = 2$ ms $g_{NMDA} = 0.327$ nS $\tau_{NMDA,rise} = 2$ ms	$\tau_m = 20$ ms $g_{GABA} = 1.2875$ nS $\tau_{GABA} = 10$ ms
Network parameters			
$\omega_+ = 2.1$ $N_E = 800$	$\omega_- = 0.877$ $N_I = 200$	$\omega_1 = 0.877$ $N_{ext} = 800$	$\omega_b/\omega_f = 1/3$ $\lambda_{ext} = 3.0$ Hz/synapse

TABLE 2. Synaptic connection strengths between the different pools D1, D2, NS and Inh in Net 1 (N1) and Net 2 (N2)

	N1 NS	N1 Inh	N1 D1	N1 D2	N2 NS	N2 Inh	N2 D1	N2 D2
N1 NS	1	1	1	1	0	0	0	0
N1 Inh	1	1	1	1	0	0	0	0
N1 D1	ω_-	1	ω_+	ω_-	0	0	ω_f	ω_{fw}
N1 D2	ω_-	1	ω_-	ω_+	0	0	ω_{fw}	ω_f
N2 NS	0	0	0	0	1	1	1	1
N2 Inh	0	0	0	0	1	1	1	1
N2 D1	0	0	ω_b	ω_{bw}	ω_-	1	ω_+	ω_-
N2 D2	0	0	ω_{bw}	ω_b	ω_-	1	ω_-	ω_+

The strengths are read from row to column. NS, nonspecific excitatory; Inh, inhibitory.

The integrate-and-fire network is modelled using the general framework, described elsewhere, which has a mean-field equivalent (Brunel & Wang, 2001; Wang, 2002; Deco & Rolls, 2006; Rolls & Deco, 2010). The external input λ_{ext} is a Poisson spike train that connects independently to all neurons in the network via 800 synapses onto each neuron, each reflecting firing at 3 Hz to simulate the effect of spontaneous activity in the cortex. The network is fully connected and has recurrent collateral synapses within Net 1 and Net 2 that are separate. Net 1 and Net 2 have separate populations of inhibitory neurons to ensure that the networks can oscillate separately if the weights ω_f and ω_b are zero.

Gamma oscillations in a network with excitatory and inhibitory neurons are generated through a pyramidal–interneuron feedback loop (Traub *et al.*, 1997; Brunel & Wang, 2003). Pyramidal neurons excite interneurons, and interneurons in turn send inhibition back onto pyramidal cells. The population frequency is determined by the sum of excitatory and inhibitory lags. The recurrent excitatory connections tend to decrease the oscillation frequency (as compared to only excitatory–inhibitory and inhibitory–excitatory connections) as they tend to prolong the positive phase in each cycle. In our network we can therefore generate and control the oscillations in the gamma frequency-band by adjusting the AMPA and NMDA receptor-activated conductances (g_{AMPA} and g_{NMDA}). For example, increasing g_{AMPA} and decreasing g_{NMDA} shifts the balance in the network towards fast excitation (AMPA) and slow inhibition (GABA) and thus increases the gamma frequency-band oscillations. The conductances in our network were varied according to the following rule: $g_{NMDA} = g_{NMDA} (1 - \delta)$ and $g_{AMPA} = g_{AMPA} (1 + 10\delta)$. We refer to the parameter δ as the g_{AMPA}/g_{NMDA} modification ratio. The factor 10 stems from the fact that near the firing threshold the ratio of NMDA : AMPA components becomes 10 in terms of charge entry, as stated in Brunel & Wang

(2001). Therefore, in order not to change the spontaneous firing rate state, a decrease in g_{NMDA} is compensated by a ten-fold increase in g_{AMPA} . All recurrent conductances (both inhibitory and excitatory) were modified according to this rule. Both Net 1 and Net 2 were set up to have gamma oscillations by altering the AMPA to NMDA ratio modification factor δ from its default value of 0 for the NMDA case to a value of 0.1 for the AMPA case, with the normal default values for the g_{AMPA} and g_{NMDA} conductances shown in Table 1, as this alteration has been shown to produce good gamma oscillations in this network (Buehlmann & Deco, 2010). We refer to the default conductances shown in Table 1 as the NMDA case, and to the $\delta = 0.1$ ratio modification factor case, where the g_{AMPA} is doubled and the g_{NMDA} is reduced to 0.9 of the values shown in Table 1, as the AMPA case.

Implementation of the integrate-and-fire attractor neuronal network model of information transmission

The probabilistic decision-making network we used is a spiking neuronal network model with a mean-field equivalent (Wang, 2002), but instead set to operate with parameters determined by a mean-field analysis that ensures that the spontaneous firing rate state is stable even when the decision cues are applied, so that it is only the noise that provokes a transition to a high firing rate attractor state (Deco *et al.*, 2012), allowing the effects of the noise to be clearly measured (Deco & Rolls, 2006; Rolls & Deco, 2010; Deco *et al.*, 2012). The reasons for using this particular integrate-and-fire spiking attractor network model are (i) that this is an established model with a mean-field equivalent allowing mathematical analysis, (ii) that many studies of short-term memory, decision-making and attention have been performed with this model which captures many aspects of experimental data (in a number of cases because, for example, NMDA receptors are included) and (iii) that

it captures many aspects of cortical dynamics well (Brunel & Wang, 2001; Wang, 2002, 2008; Deco & Rolls, 2005b, 2006; Loh *et al.*, 2007; Buehlmann & Deco, 2008; Rolls *et al.*, 2008, 2010a,b; Rolls & Deco, 2010; Smerieri *et al.*, 2010).

Each separate attractor network is fully connected and consists of separate populations of excitatory and inhibitory neurons as shown in Fig. 1. Two subpopulations of the excitatory neurons are referred to as decision pools, 'D1' and 'D2'. The decision pools each encode a decision to one of the stimuli, and receive as decision-related inputs for example λ_1 and λ_2 for Net 1 (Fig. 1). The remaining excitatory neurons are called the 'nonspecific' neurons, and do not respond to the decision-making stimuli used, but do allow a given sparseness of the representation of the decision-attractors to be achieved. These neurons might in the brain respond to different stimuli, decisions or memories.

A description of the network follows, and we further provide a description according to the recommendations of Nordlie *et al.* (2009) in Data S1.

In our simulations, each net contained $N = 1000$ neurons, with $N_E = 0.8 N$ excitatory neurons, and $N_I = 0.2 N$ inhibitory neurons. The two decision pools are equal-sized subpopulations with the proportion of the excitatory neurons in a decision pool, or the sparseness of the representation with binary encoding, $f = 0.1$, resulting in the number of neurons in a decision pool $N_E f = 80$. The neuron pools are non-overlapping, meaning that the neurons in each pool belong to one pool only.

We structured the network by establishing the strength of interactions between pools to take values that could occur through a process of associative long-term potentiation and long-term depression. Neurons that respond to the same stimulus, or in other words ones that are in the same decision pool, will have stronger connections. The connection strength between neurons will be weaker if they respond to different stimuli. The synaptic weights are set effectively by the presynaptic and postsynaptic firing rates reflecting associative connectivity (Rolls, 2008b). Neurons in the same decision pool are connected to each other with a strong average weight ω_+ , and are connected to neurons in the other excitatory pools with a weak average weight ω_- . All other synaptic weights within a pool are set to unity. Using a mean-field analysis (Deco & Rolls, 2006), we chose ω_+ to be 2.1 and ω_- to be 0.877 to achieve a stable spontaneous state (in the absence of noise) even when the decision cues were being applied, and stable high firing-rate decision states. In particular, $w_- = 0.8 - f_{D1} w_+ / 0.8 - f_{D1}$ where f_{D1} is the fraction of neurons in a specific excitatory decision-making pool such as pool D1, and in our case is 0.08 (Brunel & Wang, 2001; Wang, 2002; Deco & Rolls, 2006; Loh *et al.*, 2007; Rolls & Deco, 2010).

The connection strengths between the two networks are included in Table 2, which provides a complete specification of all the connection strengths in the network. The D1 pools of the two networks are connected by strengths of ω_f . The same values were used for the connection strengths between the D2 pools of the two networks. This value was altered parametrically as part of the investigations described here. The corresponding backward connections ω_b were always set to 1/3 of this value to reflect the anatomy of the connectivity (Rolls, 2008b; Section 1.11, pp 31–36). In addition, the D1 and the D2 pools in the first and second networks had weaker connection strengths of ω_{fw} in the forward direction, and 1/3 of this in the backward direction ω_{bw} , scaled to be 1/10 of the value of the connections ω_f and ω_b respectively to model the weak connections expected as a result of associative learning between the non-corresponding pools in two connected networks, following exactly Buehlmann & Deco (2010).

Neuron model

Neurons in our network use integrate-and-fire dynamics (Knight, 2000; Brunel & Wang, 2001; Wang, 2002; Burkitt, 2006; Deco & Rolls, 2006; Rolls & Deco, 2010) to describe the membrane potential of neurons. We chose biologically realistic constants to obtain firing rates that are similar to experimental measurements of actual neural activity. Integrate-and-fire neurons integrate synaptic current into a membrane potential, and then fire when the membrane potential reaches a voltage threshold. The equation that governs the membrane potential of a neuron V_i is given by

$$C_m \frac{dV_i(t)}{dt} = -g_m(V_i(t) - V_L) - I_{\text{syn}}(t), \quad (1)$$

where C_m is the membrane capacitance, g_m is the leak conductance, V_L is the leak reversal potential and I_{syn} is the total synaptic input. A spike is produced by a neuron when its membrane potential exceeds a threshold $V_{\text{thr}} = -50$ mV and its membrane potential is reset to a value $V_{\text{reset}} = -55$ mV. Neurons are held at V_{reset} for a refractory period τ_{rp} immediately following a spike.

Synapses

The synaptic current flowing into each neuron is described in terms of neurotransmitter components. The four families of receptors used were GABA, NMDA, AMPA_{rec} (from the recurrent collateral connections) and AMPA_{ext} (from external connections). The neurotransmitters released from a presynaptic excitatory neuron act through AMPA and NMDA receptors, while inhibitory neurons activate ion channels through GABA receptors. Each neuron in the network has $C_{\text{ext}} = 800$ external synapses that deliver input information and background spontaneous firing from other parts of the brain. Each neuron receives via each of these 800 synaptic external inputs a spike train modelled by a Poisson process with rate 3.0 Hz, making the total external input 2400 Hz per neuron.

The synaptic current is given by a sum of glutamatergic-, AMPA ($I_{\text{AMPA,rec}}$ -) and NMDA ($I_{\text{NMDA,rec}}$ -) mediated currents from the excitatory recurrent collateral connections, an AMPA ($I_{\text{AMPA,ext}}$ -) mediated external excitatory current and an inhibitory GABAergic current (I_{GABA}):

$$I_{\text{syn}}(t) = I_{\text{AMPA,ext}}(t) + I_{\text{AMPA,rec}}(t) + I_{\text{NMDA,rec}}(t) + I_{\text{GABA}}(t) \quad (2)$$

in which

$$I_{\text{AMPA,ext}}(t) = g_{\text{AMPA,ext}}(V(t) - V_E) \sum_{j=1}^{C_{\text{ext}}} S_j^{\text{AMPA,ext}}(t) \quad (3)$$

$$I_{\text{AMPA,rec}}(t) = g_{\text{AMPA,rec}}(V(t) - V_E) \sum_{j=1}^{C_E} w_j S_j^{\text{AMPA,rec}}(t) \quad (4)$$

$$I_{\text{NMDA,rec}}(t) = \frac{g_{\text{NMDA}}(V(t) - V_E)}{1 + [\text{Mg}^{++}] \exp(-0.062V(t))/3.57} \times \sum_{j=1}^{C_E} w_j s_j^{\text{NMDA}}(t) \quad (5)$$

$$I_{\text{GABA}}(t) = g_{\text{GABA}}(V(t) - V_I) \sum_{j=1}^{C_I} s_j^{\text{GABA}}(t), \quad (6)$$

where V_E and V_I are reversal potentials for excitatory and inhibitory PSPs, the g terms represent synaptic conductances, s_j are the fractions of open synaptically activated ion channels at synapse j , and weights

ω_j represent the structure of the synaptic connections. (The index j above refers to different synapses, external, recurrent, AMPA, NMDA, GABA etc. as indicated.)

Postsynaptic potentials are generated by the opening of channels triggered by the action potential of the presynaptic neuron. As mentioned above, the dynamics of these synaptically activated ion channels are described by the gating variables s_j . The dynamics of these variables are given by

$$\frac{ds_j^{\text{AMPA}}(t)}{dt} = -\frac{s_j^{\text{AMPA}}(t)}{\tau_{\text{AMPA}}} + \sum_k \delta(t - t_j^k) \quad (7)$$

$$\frac{ds_j^{\text{NMDA}}(t)}{dt} = -\frac{s_j^{\text{NMDA}}(t)}{\tau_{\text{NMDA,decay}}} + \alpha x_j(t)(1 - s_j^{\text{NMDA}}(t)) \quad (8)$$

$$\frac{dx_j(t)}{dt} = -\frac{x_j(t)}{\tau_{\text{NMDA,rise}}} + \sum_k \delta(t - t_j^k) \quad (9)$$

$$\frac{ds_j^{\text{GABA}}(t)}{dt} = -\frac{s_j^{\text{GABA}}(t)}{\tau_{\text{GABA}}} + \sum_k \delta(t - t_j^k) \quad (10)$$

where the sums over k represent a sum over spikes formulated as δ -Peaks ($\delta(t)$) emitted by presynaptic neuron j at time t_j^k .

The constants used in the simulations are shown in Table 1.

Simulation regime

The network was simulated numerically using a second order Runge–Kutta algorithm step with an integration step $dt = 0.02$ ms for a time period of 4 s. First there was a 1-s baseline period of spontaneous activity in which $\lambda_{\text{ext}} = 3.0$ Hz for each of the 800 external synapses onto each neuron. At time = 1000 ms there was then a 3-s decision period in which the decision stimuli were applied by increasing the firing rates in Net 1 for the 800 external input synapses on each of the neurons in the two decision pools to $\lambda_1 = 3.11$ Hz and $\lambda_2 = 2.99$ Hz. This caused Net 1 to reliably enter a decision attractor with pool 1 winning, and firing at a high firing rate with a typical latency of 500 ms. Also at time = 1000 ms, for Net 2 λ_3 and λ_4 were increased to 3.06 Hz, to facilitate the making of a decision in Net 2. Which decision was made in Net 2 was influenced by the firing in Net 1 pool 1 and by the net interconnection weights ω_f and ω_b between pools N1D1 and N2D2 (see Fig. 1). If the interconnection weights were zero, the parameters were such that a decision was eventually taken in Net 2, but the decision was at chance. This equal and small increase in λ_3 and λ_4 can be thought of as a nonspecific contribution to the input to Net 2, which is sometimes found in the cortex (but not typically in the inferior temporal visual cortex, the insular taste cortex, the orbitofrontal cortex, the cingulate cortex or the hippocampus; Rolls & Treves, 2011; Rolls, 2008b) and is sometimes modelled (Wang, 2002; Albantakis & Deco, 2009).

During the decision period, the noise in the network, and the increased firing rate bias functioning as a decision cue to each decision pool of neurons, causes one of the decision populations of neurons to jump to a high firing rate attractor state with the assistance of the positive feedback in the recurrent collaterals. This high firing inhibits, through the inhibitory interneurons, the other decision population of neurons. There is thus a single winning population on each trial, and which of the two populations wins on a particular trial is determined by the statistical fluctuations in the firing rates of the neurons in each decision population.

Analyses

Spectral analyses

We performed spectral analyses as described by Bendat & Piersol (2010) to analyse the oscillations and possible synchrony in the network. The analyses are described using their notation, and were implemented in MATLAB (version 2010a) using the cpsd function with the default values for the windowing and data sections to ensure that reliable averaged estimates were obtained on single trials. (We do not show \wedge symbols in the following to simplify the notation, as these averages were always used.) The number of points in the fast Fourier transform was set for the analyses described to 256, and we checked carefully that the magnitudes and phases obtained were not altered if smaller values of 128 or 64 were used. The data for each analysis consisted of 512 ms of local field potential (LFP) data (defined below) with 1-ms spacing. The data were obtained on each trial in a time period that started 12 ms before the decision in Net 2, unless otherwise stated (as oscillations were not present in Net 2 before this time, and this time was when the decision was being made). The finding that gamma oscillations are not present during spontaneous firing, and only start in Net 2 when the neurons increase their firing rates, is illustrated by the single-trial type of analysis shown in Fig. 4. However, when the Net 2 D1 neurons selectively increase their firing rates, the decision has effectively been taken; that is, the bifurcation has been crossed. This is one of the implications of the investigations described here – great care has to be taken using single-trial analyses with neurophysiological data to measure exactly when the gamma oscillations start, and also when any synchrony starts that may be present, in relation to the time of the decision or more generally of the information transmission.

We computed the power spectral density (PSD) [$G_x(f)$ for Net 1 Pool 1, and $G_y(f)$ for the winning pool in Net 2. We computed the cross-spectral density [$G_{xy}(f) = C_{xy}(f) - jQ_{xy}(f)$], where the real part $C_{xy}(f)$ is the coincident spectral density function, and the imaginary part $Q_{xy}(f)$ is the quadrature spectral density function. In the graphs we plot the magnitude of the cross-spectral density magnitude (CSM), $|G_{xy}(f)|$, as

$$|G_{xy}(f)| = \sqrt{C_{xy}^2(f) + Q_{xy}^2(f)} \quad (11)$$

and the phase as

$$\theta_{xy}(f) = \tan^{-1} \left[\frac{Q_{xy}(f)}{C_{xy}(f)} \right]. \quad (12)$$

We note that synchrony is a state in which there is a fixed phase in the activity of the two systems (e.g. neural populations), that is, when they are phase-locked. (The phase-locking need not be at zero phase.)

The coherence was calculated as

$$\gamma_{xy}^2 = \frac{|G_{xy}(f)|^2}{G_x(f)G_y(f)}. \quad (13)$$

This makes it clear that one can define an un-normalized coherence measure as the square of the magnitude of the cross-spectral magnitude, i.e. as $|G_{xy}(f)|^2$.

The above analyses provided the quantitative data for the conclusions reached. However, to visualise the time-course of the spectral changes within a trial, to help determine the time within a trial in which to perform the spectral analyses just described, we

also utilized Slepian multi-taper methods for spectrograms (i.e. spectral estimation as a function of time) (Fries *et al.*, 2008; Mazzoni *et al.*, 2008). We used an optimal family of orthogonal tapers given by the discrete prolate spheroid sequences (Slepian functions) as described elsewhere (Fries *et al.*, 2008; Mazzoni *et al.*, 2008), building on the MATLAB implementation of Partha Mitra modified by Ken Harris and made available under the GNU GPL at <http://neuromat.googlecode.com/svn/trunk/spikeMat/tools.ext/>. The length of the moving window was 256 ms. Examples are shown in Figs 4 and 11.

Spike-triggered average (STA) and cross-STA

We calculated the STA of the LFP within a network, as this is found neurophysiologically to be a sensitive measure of oscillations. We also calculated the cross-STA between for example the spikes in Net 1 D1 and the LFP in Net 2 D1, as the cross-STA is a sensitive measure of synchrony between neuronal populations (Gregoriou *et al.*, 2009).

STAs were calculated by averaging LFP segments ± 50 ms around every recorded spike. This was calculated in the same 512-ms time window used for the spectral analyses. To display more clearly the average relative phase of spikes, the STA was smoothed with a 5-point smooth. The cross-STA was calculated in an analogous way. The surrogate for the LFP was the sum of the absolute values of the AMPA and GABA currents into a neuron in the pool being considered (averaged across all the neurons in the pool), as the LFPs are thought to reflect currents such as these (Mazzoni *et al.*, 2008). We checked that the conclusions were not affected if the absolute values of the NMDA currents were included as well.

The neuronal firing rates for each neuronal population were calculated as the average across a population of the firing rate in 50-ms sliding bins.

Mutual information analyses

The information transmission from Net 1 (pool N1D1) to Net 2 (pool N2D1) was measured by the Shannon mutual information, as described in more detail elsewhere (Rolls, 2008b; Rolls & Treves, 2011). In the simulations where we have an attractor state reached in Net 2 (measured by the firing rates being 10 spikes/s higher in one of the decision pools than the other in a 500-ms period starting at the time when the firing rates diverged in N2D1 and N2D2), we can measure the mutual information between the stimulus s applied to Net 1, and the attractor state reached in Net 2, which we denote as s' . In Net 1, the attractor that wins (pool D1 or D2) was set to be D1 by setting input stimulus λ_1 to 3.11 and λ_2 to 2.99 Hz per external synapse (at the end of the spontaneous firing period in which both had been 3.00 Hz per external synapse), where there are $N_{\text{ext}} = 800$ synapses per neuron). For Net 2, information transmission is good when N2D1 enters a high firing rate attractor state $s' = 1$ when s is 1. We measure the mutual information between the input stimuli s and the state reached in Net 2, s' .

More formally, we define the stimuli or symbols in N1D1 as s drawn from the set S , and in N2D1 as s' drawn from the set S' . Prior to reception of s' , the probability of the input symbol s was $P(s)$. This is the *a priori* probability of s . After reception of s' , the probability that the input symbol was s becomes $P(s|s')$, the conditional probability that s was sent given that s' was received. This is the *a posteriori* probability of s . The difference between the *a priori* and *a posteriori* uncertainties measures the gain of information due to the reception of s' . Once averaged across the values of both symbols s and s' , this is the mutual information

$$I(S, S') = \sum_{s, s'} P(s, s') \{ \log_2[1/P(s)] - \log_2[1/P(s|s')] \} \quad (14)$$

$$= \sum_{s, s'} P(s, s') \log_2[P(s|s')/P(s)]. \quad (15)$$

MATLAB routines in the Information Theory Toolbox v1.0 were used (<http://www.mathworks.com/matlabcentral/fileexchange/17993-information-theory-toolbox-v1-0>). The decision time was measured on each trial as the difference in the latency for Net 1 to reach its attractor state and Net 2 to reach its attractor state. The criterion for being in an attractor state was that the firing rate in one of the decision pools (D1 vs. D2) had to be > 10 spikes/s on average for each neuron than in the other pool, in a 500-ms period.

In the simulations where we set the parameters so that a high firing rate attractor state was not reached in Net 2 ($\omega_{2+} = 1.3$), the mutual information between the stimulus s within the set S applied to Net 1 and the firing rates r from the set R in Net 2 of N2D1 and N2D2 was measured in the manner described in detail elsewhere (Rolls *et al.*, 1997b; Rolls, 2008b; Rolls & Treves, 2011) as follows – $I(S;R)$

$$I(S, R) = \sum_{s, r} P(s, r) \log_2 \frac{P(s, r)}{P(s)P(r)}. \quad (16)$$

The analytic bias correction procedure (Treves & Panzeri, 1995; Panzeri & Treves, 1996) was applied as normal (Rolls *et al.*, 1997b).

For these simulations where there was no attractor in Net 2, we also used a decoding procedure (described in detail elsewhere; Rolls *et al.*, 1997a; Rolls, 2008b; Rolls & Treves, 2011) whereby the firing rate in N2D1 vs. N2D2 on each trial was used to effectively identify the most likely stimulus s' which had been presented to the network. s' was decoded as 1 if the firing rate of N2D1 was higher than N2D2, and as 2 if the firing rate of N2D2 was higher than N2D1. The information was measured using Eqn 15. The firing rate in this case was measured in a 500-ms period of 1500–2000 ms on each trial, that is, starting at the time that Net 1 was in its high firing rate attractor state for pool N1D1, allowing the influence of this on the firing rates of pools N2D1 and N2D2 to be measured. This is maximum likelihood decoding (Rolls *et al.*, 1997a; Rolls, 2008b; Rolls & Treves, 2011), and allows the percentage correct to be measured (in this case as the percentage of trials on which Net 2 was in a corresponding state to that in Net 1). The latency of the response in Net 2 was measured in this case by the first bin in which a running t -test with 10 bins each of 50 ms of firing rates from N2D1 and N2D2 first became significant ($P < 0.05$), minus the actual time on that trial at which Net 1 reached its decision. The decoded information measure can be high because the estimated stimulus s' on each trial can be decoded based on which pool, N2D1 or N2D2, has a higher rate on that particular trial, independently of any small fluctuations in the average firing rate from trial to trial. In contrast, measuring the information from Eqn 16 gives smaller values in the present application, because it utilizes probability distributions assessed over many trials, and thus reflects the trial-by-trial variability in the average values of the firing rates on different trials measured within a given time window.

Transfer entropy

One measure of the mutual influence between two neuronal groups is quantified as the Spearman rank correlation coefficient of the spectral power in the gamma range (50–80 Hz for our simulations) in the two groups (Womelsdorf *et al.*, 2007). We measured this, and found similar correlations, with a peak at 0 phase lag, to those described by

Buehlmann & Deco (2010) with $\omega_f = 0.45$. An interpretation is that the oscillations are stronger in the two networks when they are in phase.

The Spearman rank correlation is a nonparametric measure of correlation which makes no assumptions about normality or linearity of the data. However, it is a symmetric measure and therefore fails to measure directionality of the flow of influence. To overcome this limitation we also use transfer entropy (Schreiber, 2000), which enables us to distinguish between shared and transported information. Transfer entropy measures the deviation from the following generalized Markov property:

$$p(x_{t+1}|x_t^k) = p(x_{t+1}|x_t^k, y^l - t), \quad (17)$$

where p is the transition probability and k and l are the dimensions of the delay vectors. x_t and y_t are the time series of the signal. We write x_t and y_t instead of $x(t)$ and $y(t)$, respectively, for better readability. If the deviation is small, then Y has no relevance for the transmission probability of X . The incorrectness of this assumption can be quantified by the Kullback entropy

$$T_{y \rightarrow x} = \sum_t p(x_{t+1}, x_t^k, y_t^l) \log_2 \frac{p(x_{t+1}|x_t^k, y_t^l)}{p(x_{t+1}|x_t^k)}. \quad (18)$$

In other words, transfer entropy represents the information about a future observation of variable x_t obtained from the simultaneous observation of past values of both x_t and y_t , after discarding the information about the future of x_t obtained from the past of x_t alone (Ishiguro *et al.*, 2008). For computational reasons, we set $k = l = 1$. The conditional probabilities required in Eqn 18 were calculated from the joint probabilities. We approximate the joint probabilities by coarse-graining the continuous state space at resolution r and using the histograms of the embedding vector (naive histogram technique; Lungarella *et al.*, 2007).

When the available data are limited (number of samples $N < 500$) and the coupling between the time series is small, transfer entropy suffers from a finite-sample effect, in particular for small resolution ($r < 0.05$), which makes the assessment of the significance of the obtained values difficult (Lungarella *et al.*, 2007). However, for all our simulations $N = 512$ and $r > 0.05$, so we can assume that the finite-sample issue affects our results only to a minor extent. We present raw values of the transfer entropy calculated in this way, but estimated the correction needed based on transfer entropy measures in unconnected oscillating networks. The value was 0.16 bits, and this may be subtracted as a correction from the values reported in this paper. We note that transfer entropy is similar in its intent to Granger causality analysis (Ishiguro *et al.*, 2008; Ge *et al.*, 2012). We calculated the transfer entropy between the multiple neuron activity (MUA; see next) in the two neuronal pools.

From our spiking simulations we calculated the multi-unit activity (MUA) to analyze our simulations, in order to be able to compare our results directly with neurophysiological experiments. To simulate the MUA, we used the 80 neurons in each of the selective pools. This point process data was converted to a time series by binning the spikes in windows of 5 ms. The binning window was shifted in steps of 1 ms. The time-series was then normalized to zero mean and unit variance. We use the normalized time-series to estimate the transfer entropy and power spectrum. Normalization was applied to rule out the possible influence of rate changes on these two measures. Both measures were made in a 512-ms window starting at the time that the decision was made in Net 2.

The transfer entropy analyses provide evidence on influences of the oscillations in Net 1 on Net 2 and vice versa. This is possible because the time window is short, 5 ms. The transfer entropy analyses do not measure how the information about which stimulus was presented to Net 1 is reflected in the decision made by Net 2, which instead is measured by the Shannon Information measures described above (Eqns 15 and 16) which measures whether N2D1 or N2D2 enters a high firing rate attractor state (and that is measured by whether the firing rates of N2D1 are greater than those of N2D2 or vice versa by 10 spikes/s on average for each neuron in a pool during a 500-ms period).

Results

Information transmission between two coupled networks

A single trial of a simulation for the AMPA case (prone to gamma oscillations) is shown in Fig. 2 to illustrate the information transmission from Net 1 to Net 2. This illustrates that after a 1-s period of spontaneous activity, the decision cues were applied to Net 1, which took the correct decision that Net 1 should win, with a latency of ~ 400 ms. The forward connection weights ω_f from pool N1D1 to pool N2D1 in this case were 0.03, and these were sufficiently strong for information to be transmitted to Net 2 pool D1 (N2D1) and for it then to win the competition in Net 2 and enter a decision attractor state with a high firing rate. Figure 2B shows the average (over 50 ms) of the firing rates of the neurons in the D1 pools of both networks. (The rapid increase in rate from a mean of 3 spikes/s in the spontaneous period to ~ 75 spikes/s when a decision has been made illustrates that an increase by 10 spikes/s from the spontaneous rate is a good criterion for a decision.) The spiking nature of the activity is illustrated in the rastergrams in Fig. 2A. The spectral analyses for the same trial are illustrated in Fig. 2C. The PSD for the local field potential in Net 1 D1 showed that there is no gamma activity in the spontaneous period, when the mean firing rates of the neurons in the excitatory neuron pools is 3 spikes/s. The power spectral density only increased in the gamma band when the D1 neurons started to fire with high firing rates in response to their inputs, reflecting what is found neurophysiologically (Fries *et al.*, 2008). Similarly, the PSD for the local field potential in Net 2 D1 showed that there is no gamma activity in the spontaneous period, when the mean firing rates of the neurons in the excitatory neuron pools is 3 spikes/s. The power spectral density only increased in the gamma band when the Net 2 D1 neurons started to fire with high firing rates in response to the inputs received from Net 1. This immediately raises a fundamental question – how could oscillations contribute to the information transmission if they do not become established until information transmission has increased the firing rates? Next, Fig. 2C shows that the coherence between the N1D1 and N2D1 populations remained low throughout the trial. This indicates that although both N1D1 and N2D1 had gamma oscillations when their firing rates were high (as shown by their PSDs), the oscillations were without any fixed phase relationship. (A case for comparison which does show coherence building up is in Fig. 3A, the AMPA case with $\omega_f = 0.45$.) Similarly, the phaseogram at the bottom of Fig. 2C also shows no fixed phase in the gamma band between the gamma oscillations in N1D1 and N2D1. (Again, a case for comparison which does show phase-locking is in Fig. 3A, the AMPA case with $\omega_f = 0.45$.) The generic results shown in Fig. 2 are prototypical for the operation of the networks, confirmed over thousands of trials with the averaged data illustrated in the next few figures. First, gamma oscillations only become clearly evident when the neurons leave their spontaneous firing rate state and are driven by inputs to reach high

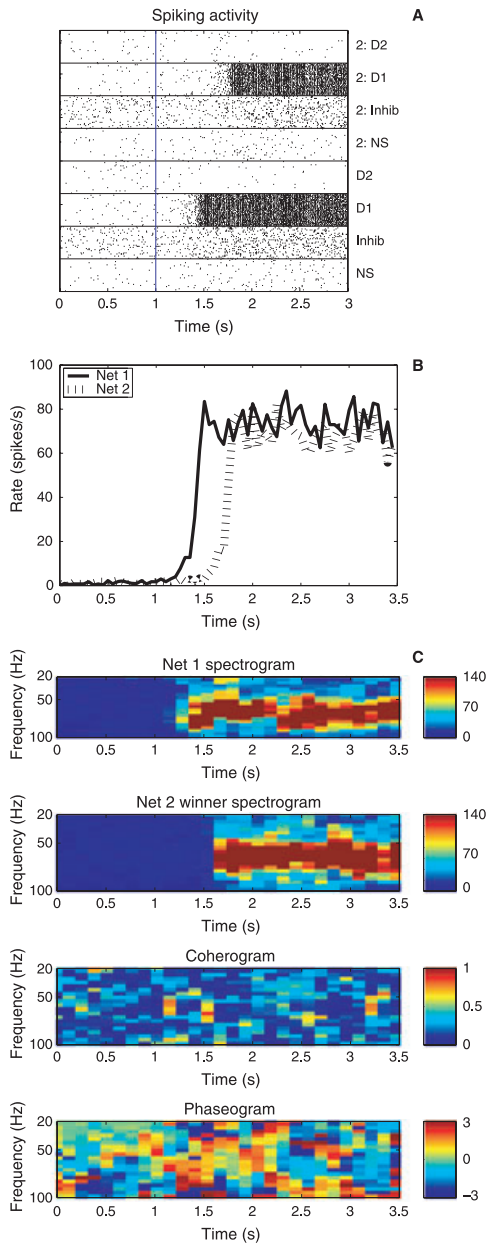
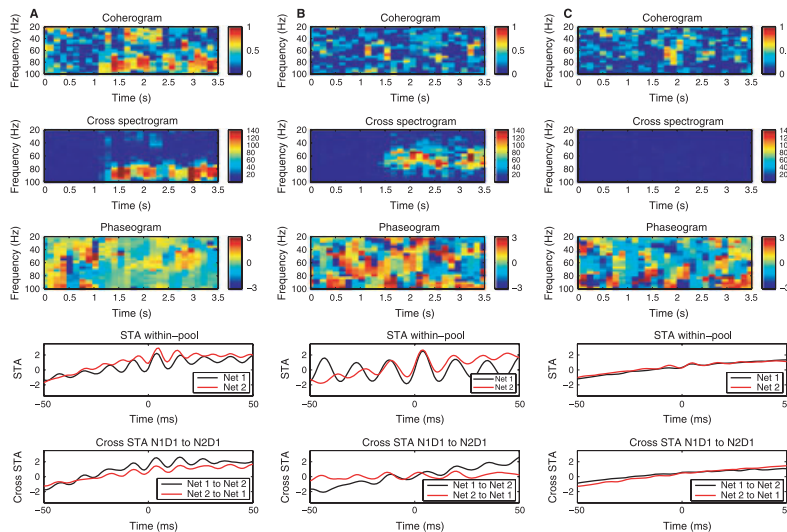


FIG. 2. A single trial of the simulation to illustrate the responses of the network in the AMPA case as a function of time. The decision cues for Net 1 were switched on at time = 1.0 s and stayed on for the remainder of the trial. $\omega_f = 0.03$. Net 1 took its decision at 1.4 s, and Net 2 at 1.7 s. (A) Rastergram, with each row of the rastergram providing the spike times for one of 30 neurons in each pool. There is a 1-s period of spontaneous activity from 0 to 1 s, and then the decision cues are applied to the neurons in pools D1 and D2 of Net 1 for the remainder of the trial. The lower four pools are for Net 1. NS, nonspecific excitatory; Inhib – inhibitory; D1, D2, the decision pools for Net 1. The upper four pools are for Net 2, with the pool names preceded by 2. (B) The firing rates of the D1 neurons in Net 1 and in Net 2. (C) The spectral analyses for this trial. (Top) Power spectral density (PSD) for the LFP in Net 1 D1. (The plots are displayed with the same arbitrary maximum of 140.) (Upper middle) PSD for the LFP in Net 2 D1 (the winning pool in Net 2). (Lower middle) Coherogram between Net 1 Pool D1 and Net 2 Pool D1. (The coherogram is the coherence which takes a value in the range 0–1 as a function of time.) (Bottom) Phaseogram between Net 1 Pool D1 and Net 2 Pool D1. (The phaseogram is the phase which takes a value in the range π to $-\pi$ radians as a function of time.)

firing rates. Second, at low values of ω_f , in the AMPA case oscillations are present in both Net 1 and Net 2 but there is no coherence between the oscillations in the two nets, no fixed phase relationship. Thus information has been transmitted from Net 1 to Net 2, and the firing rates in Net 2 D1 increased relative to those in Net 2 D2, yet this occurred without coherent oscillations between the two networks, which, as we shall see, only become established at much higher values of ω_f than are needed for information transmission from Net 1 to Net 2.

Next, further analyses of the performance found on single trials with the different types of simulation are shown in Figs 3 and 4 to illustrate the operation of the network. Then analyses based on 1000 trials for each data point are shown in Fig. 5.

Figure 3 shows LFP frequency analyses for (A) the AMPA case with $\omega_f = 0.45$, (B) the AMPA case with $\omega_f = 0.03$, and (C) the NMDA case. The spectra are for the 500-ms time period in which the decision is made. The AMPA case refers to simulations where the g_{AMPA} to g_{NMDA} factor δ was set to 0.1 to emphasize AMPA at the expense of NMDA conductances, and to promote oscillations in the gamma range. Figure 3A shows that, with $\omega_f = 0.45$, oscillations were present in both networks Net 1 and Net 2 in the gamma range of 50–100 Hz as shown by the PSD analyses (for the LFP power in Net 1 D1 and in Net 2 D1, the winning pool). (Although most of the power was in the gamma range of 50–80 Hz in most simulations, it was



found that with $\omega_f = 0.45$ the frequency was a little higher, and hence the larger frequency range was used for the quantitative analyses.) The CSM was large in the gamma range. At this value of $\omega_f = 0.45$, the phase (measured in radians) between the LFPs in Net 1 D1 and Net 2 D1 was locked close to zero. (In fact, not illustrated, the phase between the spikes in Net 1 D1 and the spikes in Net 2 D1 was very close to 0 radians, and the LFP phase illustrated corresponds to this case.) The coherence between the LFPs in Net 1 D1 and Net 2 D1 was high in the gamma range. In this case of AMPA domination and $\omega_f = 0.45$, oscillations occurred in both Net 1 and Net 2, and were locked in phase. This was a true case of synchrony and coherence.

Figure 3B shows that in the AMPA case where the g_{AMPA}/g_{NMDA} factor was set to 0.1, gamma oscillations were still present in Net 1 and Net 2 (as shown in the PSD analyses illustrated in Fig. 2C), but with the lower value of $\omega_f = 0.03$, the coherence between the LFPs in Net 1 D1 and Net 2 D1 was low in the gamma range, and so was the CSM. Moreover, the phase in the gamma range was no longer close to zero, and was very variable within a trial and across trials. These measures indicate that with this weaker value of the forward coupling, synchrony was no longer present. [We note here that on single trials the CSM (which when squared forms the non-normalized coherence) was a better measure of coherence on a single trial than the coherence measure itself, as the coherence measure is normalised by the product of the PSDs of the two time-series and so can take high and misleading values when either or both PSDs are low, that is, when either Net 1 and/or Net 2 is not oscillating. This is an important point when interpreting neurophysiological studies that report coherence. We further note that coherence indicates whether repeated estimates (in our case, measures repeated at different times in the 500-ms analysis window) of the cross-spectrum have consistent phases, but does not indicate whether the phase is zero. We further note, as shown in Fig. 5d, that the CSM measure does not take a zero value when the two networks are not coupled by synapses.]

Figure 3C shows that in the NMDA case where the g_{AMPA}/g_{NMDA} was set to its normal value for investigations of this network as shown in Table 1, no gamma oscillations were present in Net 1 and Net 2 (as shown by the PSDs). Accordingly, even with the high value of 0.45 for ω_f the CSM was very low in the gamma range and the gamma range phase was variable and not locked close to 0 (though, as in Fig. 3B, the coherence was not an especially good indicator of the lack of phase-coupling in the gamma range due to its normalisation by the PSDs). Thus there is no synchrony in the NMDA case of the two networks, and no oscillations.

These analyses were extended to show how the oscillations and synchrony if present developed during the time-course of a trial using

FIG. 4. Spectral analyses as a function of time for a single trial. (A) The AMPA case with $\omega_f = 0.45$. Net 1 took its decision at 1.3 s and Net 2 at 1.3 s. (B) The AMPA case with $\omega_f = 0.03$. This trial is the same as that shown in Fig. 2. Net 1 took its decision at 1.4 s and Net 2 at 1.7 s. (C) The NMDA case with $\omega_f = 0.45$. Net 1 took its decision at 1.3 s and Net 2 at 1.3 s. Top three rows of plots show the abscissa is the trial time in s, and the ordinate is the frequency in Hz. Top row shows coherograms between the LFPs in Net 1 D1 and Net 2 D1. Second row shows cross-spectrograms between the LFPs in Net 1 D1 and Net 2 D1. Third row shows phaseograms between the LFPs in Net 1 D1 and Net 2 D1. [In the 0.45 AMPA case shown in (A), the phase between the spikes in Net 1 D1 and Net 2 D1 was very close to 0 radians.] Fourth row shows black, the spike-triggered average (STA) between the spikes in Net 1 D1 and the LFPs in Net 1 D1; red, the STA between the spikes in Net 2 D1 and the LFPs in Net 2 D1. Bottom row shows black, the cross spike-triggered average (cross-STA) between the spikes in Net 1 D1 and the LFPs in Net 2 D1; red, the cross-STA between the spikes in Net 2 D1 and the LFPs in Net 1 D1. The STA and cross-STA analyses are for the 512-ms time period in which the decision is made.

Slepian filters. Results of typical trials are shown in Fig. 4. Figure 4A shows the analyses for the AMPA case with $\omega_f = 0.45$. On the trial illustrated, with this strong forward coupling ω_f of 0.45 (and backward coupling ω_b set to 1/3 of this as for all the results described), Net 1 took its decision at ~ 150 ms after the decision cues were applied, i.e. at

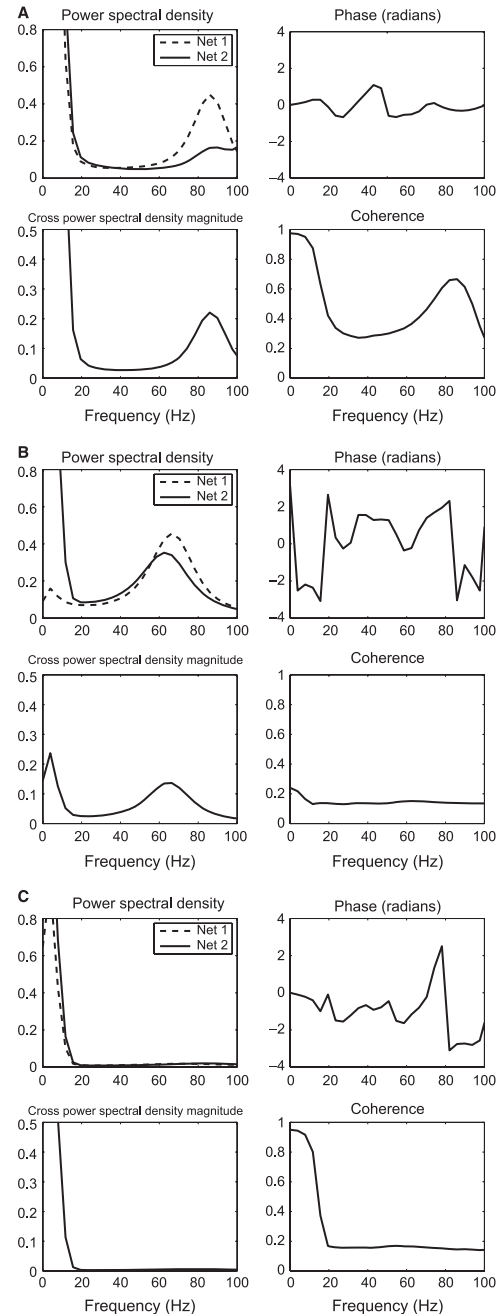


FIG. 3. Local Field Potential (LFP) frequency analyses for (A) the AMPA case with $\omega_f = 0.45$, (B) the AMPA case with $\omega_f = 0.03$, and (C) the NMDA case with $\omega_f = 0.45$. The abscissa is the frequency in Hz. The spectra are for the 500 ms time period starting when the decision is made. Each set of plots shows: Power Spectral Density = LFP power in Net 1 D1 and Net 2 D1, the winning pool. Cross-Spectral Density Magnitude (CSM) of the LFPs between N1D1 and the winning pool in Net 2. The square of this is the unnormalised coherence. Phase = phase (radians) between the LFPs in Net 1 D1 and Net 2 D1. (In the $\omega_f = 0.45$ AMPA case shown in (A), the phase between the spikes in Net 1 D1 and Net 2 D1 was very close to 0 radians.) Coherence = coherence between the LFPs in Net 1 D1 and Net 2 D1. The results are each averaged over 1000 trials, except for the phase which is for a single trial.

1150 ms into the trial, and Net 2 took its decision at approximately the same time. The cross-spectrogram for the LFP showed an increase at approximately the time of the decision, that is, when the neurons fired fast as they entered the attractor. The oscillations in each of the networks evident in the firing rates increased at approximately the same time (not illustrated), that is, the spontaneous firing rate did not support significant gamma oscillations. The coherogram also showed an increase at the decision time. (When interpreting the exact timing of events in Fig. 4, it is important to appreciate that the time window in which the Slepian filters operated was 256 ms of data, with the results plotted at the start of that time window. The values plotted at a point in time thus reflect what happened in the following 256 ms.) The phase analysis shown in Fig. 4A shows that the phase of the LFPs in Net 1 D1 and Net 2 D2 actually became locked close to 0 radians from ~ 1.4 s into the trial, that is, after the decision had been taken in both networks. The STA within Net 1 D1 (i.e. the relation between the spikes in N1D1 and the LFP in N1D1) calculated in the 500-ms period starting at the time at which the decision was taken showed a significant peak close to 0 ms, reflecting coupling between the spikes and the LFPs. (The strong oscillations are indicated by further peaks away from the central peak.) The same strong STA effect occurred in N2D1, the winning pool in Net 2. The cross-STA from Net 1 to Net 2, and vice versa, also indicate the strong phase-linked coupling between the networks. (The cross-STA from Net 1 to Net 2 shows the LFP in Net 2 D1 that is related to a spike in Net 1 D1, during the 500 ms decision period.) It is

important to note that none of the measures described showed any relation to the decision-making if they were taken in the period before Net 2 took its decision as indicated by an increase in firing rate in one of its decision pools, even immediately before.

Figure 4B shows the analyses for the AMPA case with $\omega_f = 0.03$ for a typical single trial. On this trial, Net 1 took its decision at ~ 400 ms after the decision cues were applied, i.e. at 1.4 s into the trial, and Net 2 took its decision ~ 300 ms later. (The decision time for Net 2 was thus 300 ms). The cross-spectrogram for the LFP (scaled to the same maximum as in Fig. 4A) showed a small increase in the gamma range at approximately the time of the decision in Net 2, that is, when the neurons fired fast as they entered the attractor, but the coherogram showed little change, and there was no phase-locking evident in the gamma range. The oscillations in each of the networks evident in the LFPs increased to high values in each of the networks at approximately the same time (not illustrated), and are evident in the STA analyses shown in Fig. 4B. The cross-STAs from Net 1 to Net 2 and vice versa also indicate only weak phase-linked coupling between the networks. Thus in this case, strong oscillations were present in each of the networks separately, but with this lower value of $\omega_f = 0.03$ there was no phase-locking or synchrony between the two networks Net 1 and Net 2.

Figure 4C shows the analyses for the NMDA case with $\omega_f = 0.45$ for a typical single trial. On this trial, Net 1 took its decision at ~ 300 ms after the decision cues were applied, i.e. at 1.3 s into the

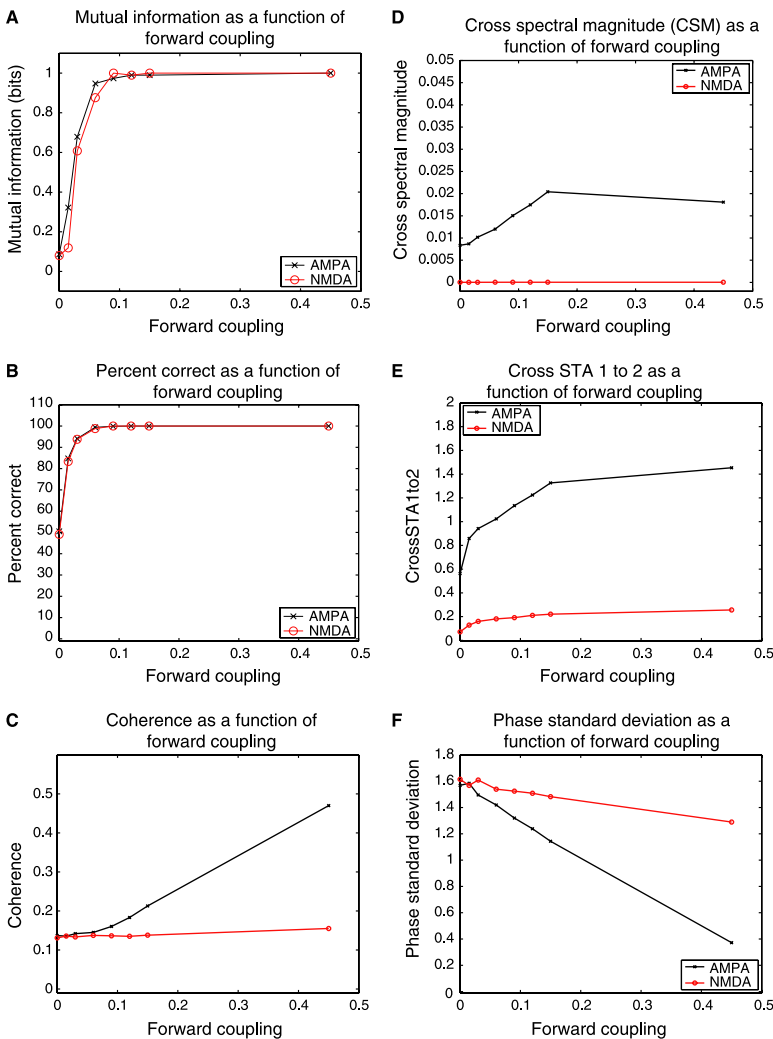


FIG. 5. Performance of the network as a function of the value of the forward coupling weight ω_f . The spectral analyses were set to include the gamma frequency-band in the range 50–100 Hz in which oscillations were induced in the networks when the g_{AMPA}/g_{NMDA} ratio was increased (the AMPA case). The NMDA case is with the normal value ratio of g_{AMPA} to g_{NMDA} as shown in Table 1. (A) Information transmission between Net 1 and Net 2. (B) Percentage correct for Net 2. (C) Coherence between Net 1 and Net 2. (D) CSM between Net 1 and Net 2. (E) Cross spike-triggered average Net 1 (spikes) to Net 2 (LFP). (F) The standard deviation of the phase in the gamma frequency-band across trials. The low standard deviation at $\omega_f = 0.45$ for the AMPA case reflects phase-locking.

trial, and Net 2 took its decision ~ 50 ms later. The cross-spectrogram for the LFP (scaled to the same maximum as in Fig. 4A) showed no effects, the coherogram showed no change, and there was no phase-locking evident in the gamma range. There were no gamma oscillations in either of the networks, and this is evident in the STA analyses shown in Fig. 4C. The cross-STAs from Net 1 to Net 2 and vice versa also indicate no phase-linked coupling between the networks. Thus in this case, no gamma oscillations were present in either of the networks separately, and even with a high value of $\omega_f = 0.45$ there was no gamma phase-locking or synchrony between the two networks Net 1 and Net 2.

The time-course analysis of the spectra based on the LFPs in Fig. 4 shows that the oscillations started in a network at approximately the time that a network took a decision for one of its attractor pools to fall into a high firing rate decision state. As the gamma oscillations were not apparent before this time, the analyses described next using 1000 trials for each data point started at the time that the second net took a decision, and were for a 500-ms period. We did perform analyses for earlier periods, including 400 ms before the decision in Net 2 was reached until 112 ms after the Net 2 decision was taken, but no gamma oscillation-related effects were found, as there were no gamma oscillations evident even in the LFPs before the decision was reached in Net 2, as illustrated in Fig. 2C. In particular, when the coherence between Net 1 and Net 2 was measured in the period before Net 2 took a decision (in fact, in the 512-ms period starting 400 ms before Net 2 responded), there was no measurable coherence different from that in uncoupled networks that could have influenced the decision in Net 2.

Consistent conclusions were reached by the transfer entropy and power correlation analyses. The transfer entropy, based on the firing rates of the N1D1 and N2 winning pools measured in the 500-ms period in which Net 2 took its decision, was high (0.30 bits) in the forward direction, and a little lower (0.28 bits) in the backward direction (consistent with the fact that ω_b was always set to $1/3$ of the value of ω_f) in the AMPA case. These transfer entropy values are consistent with those found by Buehlmann & Deco (2010), and indicate that in the system described here, after the decision has been taken, the short time-scale ongoing oscillations and firing rate fluctuations are clearly evident. The transfer entropy values were smaller when ω_f was smaller (0.015), as expected (0.23 vs. 0.25 bits for forward vs. backward). The transfer entropy values were smaller in the NMDA case (when $\omega_f = 0.45$, 0.176 and 0.182 bits for forward vs. backward), reflecting the lower gamma oscillations and therefore lower rapid-time-scale interactions between Net 1 and Net 2. The power correlation analyses (based on the LFPs) showed that during the same period the power correlation was highest for zero phase. These power correlation analyses are again consistent with those found by Buehlmann & Deco (2010), and indicate that in the system described here after the decision has been taken the short time-scale ongoing oscillations and firing rate fluctuations are clearly evident. The power correlation and STA analyses reflect what is measured in many neurophysiological experiments (Fries, 2005, 2009; Gregoriou *et al.*, 2009).

The operation of the system as a function of the forward connection strength ω_f is shown in Fig. 5. The spectral analyses were set to include the gamma frequency-band in the range 50–100 Hz in which oscillations were induced in the networks when the $g_{\text{AMPA}}/g_{\text{NMDA}}$ ratio was increased (the AMPA case). The information transmitted (Fig. 5A) and the percentage correct (Fig. 5B) increased as ω_f was increased from a low value of 0.015 up to a value of 0.09, by which value the information transmission saturated at 1 bit (perfect decision-making by Net 2) and the percentage correct saturated at 100%. The

information transmission and percentage correct curves as a function of the forward connection strength ω_f were indistinguishable for the AMPA (gamma oscillating) and NMDA (non-gamma-oscillating) cases. Results are shown for values of ω_f of 0, 0.015, 0.03, 0.045, 0.06, 0.09, 0.15 and 0.45.

Figure 5C shows that the oscillations in Net 1 and 2 in the AMPA case were almost independent as indicated by the gamma-band coherence measure for the whole range of ω_f values up to and including 0.09, the range in which the information transmission was shown to be taking place to reach saturation. Moreover, the measured coherence in this range was almost identical to that for the NMDA case (Fig. 5C). (Because coherence is normalized by the power, the values can be similar for the NMDA case without much gamma power and the AMPA case with much gamma power. The coherence provides a measure in the range 0–1 of whether there are consistent phase relations in the different samples, in this case trials, between Net 1 and Net 2. The CSM shown in Fig. 5D does reflect the non-normalized gamma power. As shown in the Methods, the square of this is the non-normalized coherence, and was a particularly useful measure on single trials in these analyses, as a high value indicated significant power in both Nets 1 and 2, as well as coherence.) In the AMPA case, the coherence only increased significantly for high values (relative to those needed for information transmission) of ω_f of 0.15 and 0.45. Also in the AMPA case, the non-normalized coherence also only increased at values of $\omega_f > 0.09$, by which value information transmission was almost perfect. The implication is that information transmission can occur in the network at much lower values of connection strength than those necessary to support coherent oscillations between the networks. It is in this sense that there is communication before coherence, that is, before the connections are sufficiently strong to support coherent oscillations.

That analysis is supported by the cross-STA between spikes in Net 1 D1 and the LFP in Net 2 D1 shown in Fig. 5E, which is a sensitive measure of synchrony between neuronal populations (Gregoriou *et al.*, 2009). The cross-STA for the AMPA case at $\omega_f = 0$ indicates what would be measured by chance, and the measure shows only a small increase for values of ω_f of 0.09 by which information transmission saturates. The major part of the increase in the cross-STA, reflecting increasing synchrony, occurs for ω_f values in the range 0.09–0.45. The cross-STA is much smaller in the NMDA case, reflecting the fact that in this case there are no clear LFP oscillations in Net 2 to be in synchrony or not with spikes in Net 1. This measure thus indicates that coupling of gamma oscillations between the networks only becomes large after information transmission has saturated (the AMPA case), and is essentially absent in the NMDA case even though information transmission is perfect.

The analysis is also supported by the phase analysis shown in Fig. 5F. The standard deviation of the phases across trials is large (close to 1.6 radians) when there is no coupling between the networks, and remains high in the NMDA case when ω_f is increased. In the AMPA case, significant phase-locking only becomes evident at the very large connection strength ω_f value of 0.45, far beyond the value of 0.015 at which significant information transmission occurs, and the value of 0.09 at which the information transmission saturates.

The decision times as a function of the forward coupling ω_f in Fig. 6A show that the major decrease in the decision time took place for values of $\omega_f \leq 0.06$. Within this range, for the AMPA condition the coherence hardly changed, as shown in Fig. 5C. Similarly, the CSM changed very little within this range of values of $\omega_f \leq 0.06$ (Fig. 6B). This is the range within which information was being transmitted between Net 1 and Net 2. At higher values of ω_f the CSM

increased in the AMPA case and the decision time decreased, as shown in Fig. 6B. However, this effect was just related to the somewhat higher firing rates that were present in the AMPA than in the NMDA case, as shown in Fig. 6C. (It is well established that factors that increase the firing rates of an attractor decision-making network decrease the decision times; Rolls *et al.*, 2010a,b). In fact, taking a particular value of the firing rate such as 60 spikes/s in Fig. 6C, it is seen that the decision time is in fact faster in the NMDA (non-oscillating) than in the AMPA (oscillating) case. Thus the presence of oscillations did not speed decision times in this set of coupled networks. Further, taking the two highest values of ω_f , 0.45 produced similarly fast decision times in the NMDA and AMPA networks (Fig. 6A) though the AMPA network, when in its synchronous firing state, had much higher firing rates (Fig. 6C). (The fact that the firing rates when in the attractor state were higher in the AMPA case indicates that the compensation for the g_{AMPA} vs. g_{NMDA} change in the AMPA-case networks described in Materials and methods, which was designed to make the spontaneous firing rates similar when the g_{AMPA}/g_{NMDA} ratio was changed, did not achieve this for the much higher firing rates when in the attractor state.) Moreover, the decision times did not depend on the oscillations *per se*, as shown by the decision times in the NMDA case, which were independent of the gamma range cross-spectral magnitude which remained close to 0 for all decision times in the NMDA case (Fig. 6B).

Further evidence that the decision times within the range of values of ω_f that influenced information transmission did not depend on coherence is provided by the phase analysis shown in Fig. 6D for $\omega_f = 0.03$. This shows for 1000 trials that the decision time was not a function of the gamma phase that happened to be present between Net 1 and Net 2.

The implication is that the speed of information transmission, and information transmission itself, do not depend on coherence or synchrony (phase-locking) between two weakly coupled attractor networks in which the coupling is nevertheless sufficiently strong to support information transmission to 100% correct between the two networks. The small increase in coherence at higher values of ω_f than 0.06, and even the phase-locking at $\omega_f = 0.45$, appear just to reflect the stronger connections between Net 1 and Net 2 after information transmission has almost saturated.

It must be emphasized that we are considering here the transmission of information about an external stimulus (λ_1) through one Net (1) to a second (Net 2). This is not what was studied in previous work in which effectively the influence of oscillations in one network on oscillations in a second network has been shown to be phase-dependent, at least at high values of ω_f (Buehlmann & Deco, 2010). Indeed, a considerable part of the literature on oscillations involving LFPs and also spiking has measured this type of influence, for example by the correlation between two networks as a function of phase (Fries, 2005, 2009). We are concerned with a different type of information transmission, about external events through brain networks, in this paper.

Information transmission when the phase between two coupled networks is externally controlled

The results described above show that the information transmission occurs at values of the coupling ω_f that are much smaller than those needed to produce marked coherence or synchrony. We were nevertheless interested in investigating whether the relative phases of Net 1 and Net 2, if coherence was present, might influence the information transmission or the decision time. We therefore ran further simulations where the external input to particular pools of neurons had a 60-Hz sine wave modulating it. The modulation had a mean value of

0 (i.e. it was a modulation and not an addition) and amplitude (peak-to-peak) equivalent to 0.4 spikes/s per synapse (in the context that the external input apart from this was typically 3.05 spikes/s per synapse). This modulation value of 0.4 spikes/s per synapse was sufficient to influence the firing rates of the neurons in a pool, and to influence the phase plots of the firing rates and the LFPs, as will be shown. This value was also chosen to be relatively small, so as not to impair the ability of the connections ω_f between the two networks to produce information transmission.

Figure 7 shows a case in which we achieved in this way phase control of the firing times of neurons in Net 1 pool 1 (N1D1) and Net 2 pool 1 (N2D1). The phase control achieved is shown in Fig. 7A (the phase applied was 180° apart) and Fig. 7C (0°). Figure 7B is a polar plot showing that the mean decision time (across 1000 trials) as a function of the relative phases achieved in the network of N1D1 vs. N2D1 did not affect the decision times. ω_f was 0.015, a value that does not saturate information transmission, so that the network is sensitive to its important parameters. There was no effect of the relative phases on either the information transmitted or percentage correct. Thus in this well controlled system of two networks, even when the phases of the two networks were locked by artificial external control firing rates applied to each network, the phase, and whether synchrony was present (as it was at 0°), had no influence on the communication between the networks. Consistent results, of the phase having no effect on decision times, were obtained with $\omega_f = 0.15$, and in this case the decision times were ~70 ms.

We did wish to test whether the phase of some neurons in the network might influence the operation of the system, a topic on which there has been much discussion in the literature (Fries *et al.*, 2001; Fries, 2009; Tiesinga & Sejnowski, 2010; Wang, 2010). We therefore were keen to test a control case to show that, in our system, phase in some parts of the network was an important factor in the operation of the system, even if phase was not important in influencing the transmission between two networks. We were able to influence the decision times of the system if we controlled the phases of the Net 2 D1 neurons relative to the Net 2 GABA (N2GABA) neurons, using the same amplitudes for the sine waves etc. as in Fig. 7. The results are shown in Fig. 8. If the 60-Hz external inputs to these two pools were in phase (0°), their firing was closely in phase, and as the phase of the external sine waves was shifted, so it was possible to shift the relative phase of the firing of N2D1 vs. N2GABA by a small amount. The phase-locking close to 0° of these two pools of neurons was associated with shorter decision times, as shown in Fig. 8, and with longer decision times when the phases of the firing were shifted. This shows that the relative phase of firing of some populations of neurons in the system can influence the processing time. In this case, the interpretation is that if the firing of the GABA neurons is shifted out of phase with the firing of the N2D1 neurons, then shunting inhibition arrives at the N2D1 neurons just when they may be about to respond with an action potential, and so this reduces the responsiveness of the N2D1 population. These experiments were performed with $\omega_f = 0.015$.

We performed another experiment to test whether the phase of the firing of N2D1 relative to N1D1 might influence the speed of information transmission between the two nets. We reasoned that any effects in the speed with which the state of Net 1 affected Net 2 might depend on both nets already oscillating and on their relative phases of coherent oscillations when a new input was applied to Net 1. To test this hypothesis, we performed the following experiment in which we started gamma oscillations in N1D1 and N2D1 with sine waves at 60 Hz applied from time = 0, and in which we

applied decision cues to N1D1 with $\lambda_1 = 3.11$ and $\lambda_2 = 2.99$ Hz per external synapse from time = 0. As shown in the rastergrams in Fig. 9a, N1D1 started firing within the first 500 ms, and the forward connections with value $\omega_f = 0.09$ from N1D1 to N2D1 started up an attractor in N2D1 by ~ 1000 ms. (The phase of firing of the N2D1 neurons relative to the N1D1 neurons was well controlled by the applied sine waves, as shown by the finding that the mean phases of the firing of N2 relative to N1 in the frequency range 50–70 Hz were close to the externally applied phase differences of 0, $\pi/4$, $\pi/2$, and $3\pi/4$.) Then at time = 2000 ms we increased the firing rate of the neurons in N1D1 (by changing λ_1 from 3.08 to 3.48 spikes/s per synapse and λ_2 from 3.00 to 2.92 spikes/s per synapse to increase the firing in N1D1; Fig. 9a). (ω_+ was 2.0, and λ_{ext} to N2D1 and N2D2 was held constant throughout each trial at 3.03 spikes/s per synapse.) Fig. 9b shows that the phase in the gamma range of N2D1 relative to N1D1 did not significantly affect the latency for an increase in firing rate in N2D1 to be found. [The latency of the change in firing rate in N2D1 was measured as the first 50-ms firing rate time bin at which the value was significantly higher ($P < 0.005$) than the firing rate in the period of time = 1650–2000 ms which immediately preceded the change in λ to increase the firing in N1D1. Typical firing rates in N2D1 were 58 spikes/s before time = 2000 ms and 64 spikes/s after the effect had become evident in N2D1.]

The implication is that, in this system, the speed at which one network can cause a change in firing rate in a second weakly connected network (typical of the cortex) is not influenced by the phase of the firing when both networks are oscillating in the gamma range.

Information transmission to a non-attractor network

The results described above have been for the case when Net 2 (and also Net 1) were decision attractor networks. We also investigated cases where Net 2 was not an attractor network, but which had firing rates that reflected information transmitted from N1D1 to N2D2.

First, we examined a case where ω_+ in Nets 1 and 2 was reduced to 1.7, insufficient to maintain a high firing rate attractor state. Under these conditions, due to the values of $\lambda_1 = 3.11$ and $\lambda_2 = 2.99$ Hz per synapse applied to N1, pool N1D1 fired at ~ 6 spikes/s and pool N1D2 at ~ 2 spikes/s. For the range of values of the connectivity between the two networks ω_f up to 0.15, pool N2D1 fired at up to 3 spikes/s and pool N2D2 at ~ 2 spikes/s. Information transmission, measured as described in Materials and methods (mutual information section) occurred as described in the attractor case, but there were no gamma oscillations in either network and thus no gamma synchrony. In further investigations in which the phase of the two networks was controlled by external sine waves applied at 60 Hz, again no effect was found on information transmission or response time (measured as described in Materials and methods).

Second, we repeated these investigations but with ω_+ in Net 1 set to 2.1 to produce a high firing rate attractor, and ω_+ in Net 2 set to 1.3 so that it did not enter a high firing rate attractor, but had rates which could reflect the large difference in the firing rates in Net 1 (typically 50 spikes/s for N1D1 and 3 spikes/s for N1D2). Gamma oscillations occurred in Net 1. When the phase of the oscillations was controlled by externally applied sine waves applied to N1D1 and N2D1, there was still no significant effect on information transmission or on response time as shown in Fig. 10. Indeed, an ANOVA on the response times for 800 trials with four phases showed $F_{3,3196} = 0.306$, $P = 0.82$. Even comparing the decision times for phase = 0° vs.

phase = 90° , $F_{1,1598} = 0.637$, $P = 0.42$. The phase control was good, as shown by the spectrograms in Fig. 11A for phase = 0° and Fig. 11B for phase = 180° . The phase was measured from the spiking, though similar effects were found when measured from LFPs. The spectral analyses show that N1D1, with its 60-Hz sine waves applied from time = 0 went into a high firing rate attractor state with much gamma power at ~ 1400 ms into the trial. The CSM between N1D1 and N2D1 was low. Two separate simulation runs (0.03a and 0.03b) with 1000 trials each were performed with $\omega_f = 0.03$, as this was within a sensitive range for information transmission, which averaged close to 0.35 bits and 82% correct. Typical mean rates for each neuron in N2D1 were 2.3 spikes/s, and in N2D2 1.9 spikes/s. The results of simulation runs of 1000 trials with $\omega_f = 0.015$ and 0.06 are also shown in Fig. 10, and the implications are similar.

Discussion

One of the important conclusions is that information transmission between coupled cortical networks may occur at values of the interconnection strengths between the networks that are much lower than those necessary to induce synchronization. This is shown by the results in Fig. 5B,C. Figure 5B shows that the percentage correct of the second network rises to very close to 100% whereas the coherence remains at the 'chance' value that is measured when there is no coupling at all between the networks ($\omega_f = 0$, the first point on the x-axis) for values of ω_f up to 0.09 (the first three data points > 0 in Fig. 5). In this sense communication occurs before coherence. The point is fully supported by the information transmission values shown in Fig. 5a. Coherent oscillations only occur when much higher values of the synaptic coupling strength between the networks is present, e.g. $\omega_f = 0.45$ (Fig. 5C). Thus information transmission between coupled networks that model pairs of interconnected networks in the same cortical area or in different cortical areas occurs at much lower values of the synaptic coupling strengths than are necessary to induce synchrony of gamma oscillations.

We emphasize that we are investigating a biologically realistic situation in which there are firing rate differences between the neuronal populations that are part of the encoding of the information to be transmitted, for differences in firing rates between different neurons are part of the normal representation of information in cortical areas including the inferior temporal visual cortex, hippocampus, orbitofrontal cortex, anterior cingulate cortex and insular taste cortex (Rolls, 2008b; Rolls & Treves, 2011). Hence, if one were to argue that coherence was only important in information transmission when there were no firing rate differences in the transmitting populations of neurons representing the different stimuli, the hypothesis would be so restrictive that it would apply to rare cases in the cerebral cortex.

Another important conclusion is that even when synchrony was artificially induced by external inputs, the information transmission between the two coupled networks and the speed of response were not influenced by the phase of their gamma oscillations (Fig. 7). In a positive control condition, we were able to show that the relative phase of the gamma oscillations between the GABA inhibitory interneurons and the excitatory cells within the *same* network did influence the decision time (Fig. 8).

Another conclusion is that the same findings and conclusions follow for neural systems that have quite different dynamics and fluctuations. In the AMPA case when there are gamma oscillations and the dynamics are fast, the result was that the information transmission between the coupled networks was not affected by the coherence in the gamma range of the two networks. In the NMDA case where the

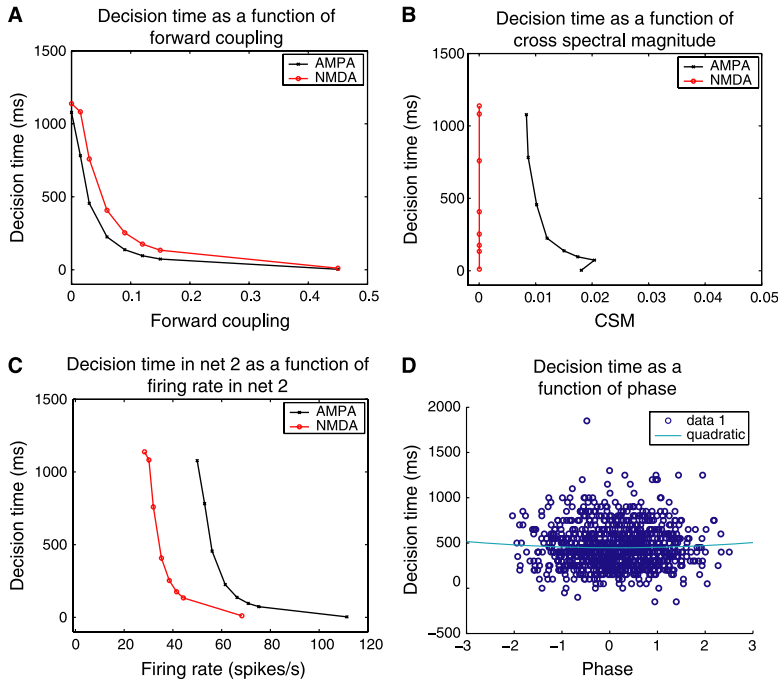


FIG. 6. Decision time for Net 2 as a function of (A) the value of the forward coupling weight ω_f , (B) the CSM and (C) the firing rate in the winning pool in Net 2. (D) The relation between the decision time and the gamma phase relation (radians) between Net 1 and Net 2 for 1000 trials with $\omega_f = 0.03$. A quadratic fit is shown.

dynamics are slower and there are no gamma oscillations, information transmission occurred in quantitatively the same way as when there were oscillations in the AMPA case, as shown by the similar percentage correct and information transmission in the AMPA and NMDA scenarios as a function of the synaptic coupling ω_f between the networks (Fig. 5).

We note that three ways have been described of producing synchrony in a single network or ‘cortical minicolumn’ (Tiesinga & Sejnowski, 2009). First, by inheritance of synchrony from previous areas via the feedforward projection; second, by activation of inhibitory networks via the interneuron gamma (ING) mechanism; and third, by activation of reciprocally connected networks of excitatory and inhibitory neurons via the pyramidal–interneuron gamma (PING) mechanism within a single network (Tiesinga & Sejnowski, 2009). However, the results of such analyses (Tiesinga & Sejnowski, 2009) apply to what happens within a single network (or minicolumn), for example within Net 2 in Fig. 1. We instead in this paper examine a different and new situation highly relevant to cortical

function, the information transmission between two networks (Net 1 and Net 2 in Fig. 1) or minicolumns.

The results found here show the way in which the information transmission between two coupled networks is influenced by the strength of the associative synaptic coupling ω_f between the two networks (Fig. 5A,B). Relatively weak synaptic connections between the two networks relative to those within the network required to maintain an attractor state are sufficient for the information transmission. Whether the network is having gamma oscillations (the AMPA dominated case) or not (the NMDA case) does not influence the information transmission (Fig. 5A,B). Thus oscillations, coherence and synchrony are not necessary for information transmission in these networks.

The system we have investigated thus operates with strong coupling within each network (e.g. within Net 1 and within Net 2) but relatively weak coupling between the two networks. This is exactly the system that applies in the cortex (Rolls & Treves, 1998; Renart *et al.*, 1999a,b), where the connections between networks must be less than in the order of 0.01 of the internal recurrent collateral strength for the two networks to have the potential to operate separately (see further Rolls & Treves, 1998; Rolls, 2008b). Consistently, in the investigations described here, information transmission between the coupled nets took place when the relative value of the inter-network connectivity to the intra-network (intra-decision-pool) connectivity was $0.015/2.1 = 0.007$. Indeed, in the phase-control experiments, it was difficult to move the phases of the oscillations between the D1, D2 and GABA neurons and LFPs within Net 1 or Net 2, due to the strong recurrent connection weights between the within-network pools of neurons. However, it was possible to move the phase of the oscillations between Net 1 and Net 2 (Fig. 7), as the connections between the two networks ω_f and ω_b were relatively much weaker.

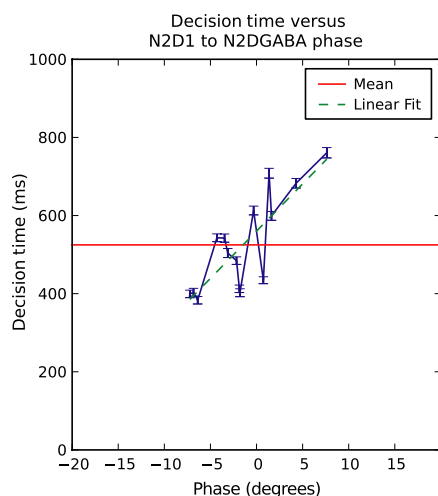


FIG. 8. Decision time with phase control. The mean decision time (ms; across 1000 trials) as a function of the relative phases (in degrees) of the firing rates in pools N2D1 and N2GABA. The phase shift was achieved by applying 60-Hz sine waves to the neurons in Net 2 pool 1 (N2D1) vs. the Net 2 GABA pool (N2GABA). ω_f was 0.015.

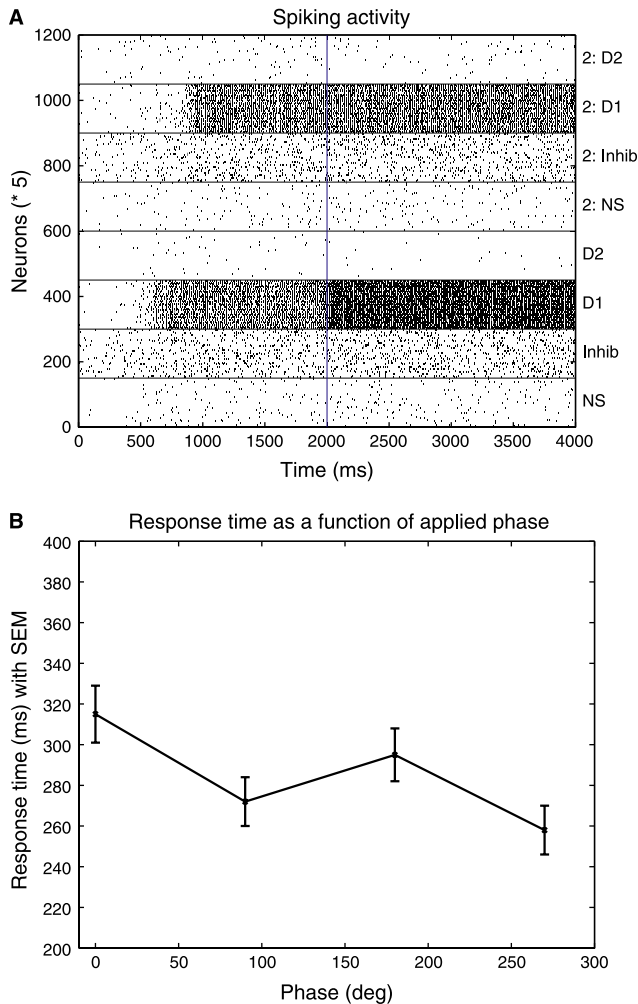


FIG. 9. The response time (\pm SEM) for Net 2 to increase its firing rate after an increase in the firing rate of Net 1 produced at time = 2000 ms. Both nets were made to oscillate by increased AMPA conductances ($\delta = 0.1$), the $\Delta\lambda = 0.04$ spikes/s per external synapse applied to Net 1, and the connections $\omega_f = 0.09$ from N1D1 to N2D2. At time = 2000 ms the firing rate in N1D1 was increased by increasing λ_1 , as shown in the rastergrams in (A). (B) The time for a change in the firing rate in Net 2 as a function of the LFP phases of Net 2 relative to Net 1 produced by externally applied sine wave modulation in the gamma range at 60 Hz.

We emphasize that even when oscillations are present (the AMPA case), phase-locking and thus synchrony only become strong at the highest value of ω_f , 0.45 (Fig. 5F) whereas information transmission has saturated at 1 bit with ω_f values of 0.09 (Fig. 5A,B). Even at $\omega_f = 0.15$ and 0.09, there is only a limited degree of phase coupling (Fig. 5f), coherence (Fig. 5C), CSM (Fig. 5D) or cross-STA (Fig. 5E). Thus information transmission saturates at much lower values of the coupling between these neural systems (Nets 1 and 2) than are needed to induce coherence and synchrony in networks that are oscillating. In this sense, ‘communication occurs before coherence’.

The implication of the findings in Fig. 6 is that the speed of information transmission (as well as information transmission itself) does not depend on coherence or synchrony (phase-locking) between two weakly coupled attractor networks in which the coupling is nevertheless sufficiently strong to support information transmission to 100% correct between the two networks. The small increase in coherence at higher values of ω_f than 0.06, and even the phase-locking

at $\omega_f = 0.45$, appear just to reflect the stronger connections between Net 1 and Net 2, after information transmission has almost saturated. Further evidence that the decision times within the range of values of ω_f that influenced information transmission did not depend on coherence is provided by the phase analysis shown in Fig. 6D for $\omega_f = 0.03$. This shows for 1000 trials that the decision time was not a function of the gamma phase that happened to be present between Net 1 and Net 2.

It must be emphasized that we are considering here the transmission of information about an external stimulus (λ_1) through one net (1) to a second (Net 2). This is different from and extends what has been found in earlier work. In that earlier work, the influence of oscillations in one network on oscillations in a second network has been shown to be phase-dependent, at least at high values of ω_f (Buehlmann & Deco, 2010). Indeed, a considerable part of the literature on oscillations involving LFPs and also spiking has measured this type of influence, for example by the power correlation between two networks as a function of phase, and by the STA (Fries, 2005, 2009). Those findings were replicated in the present findings. For example, considering the period in which a decision had just been taken, the power correlation between the LFPs in Nets 1 and 2 was maximal at zero phase, and the transfer entropy values were high, in the AMPA case. This indicates that ongoing fluctuations in the firing rates, including those produced by oscillations, are present in this network when high firing rate decision states are present in both Net 1 and Net 2. In this paper we have taken matters forward by asking a different question, whether the information transmission about external events through connected brain networks, which is prototypical of the function of cortical neuronal networks (Rolls, 2008b), is influenced by the oscillations and their phase in the coupled networks. The results of this new type of analysis presented here indicate that this type of information transmission in this prototypical case of two coupled networks is not influenced by oscillations or by their phase if oscillations are present, nor is the speed of information transmission. We believe that this is the first time this has been measured in a highly defined model system. We suggest that it will be important to measure the role of oscillations in this scenario in future in neurophysiological experiments. We note that the system we investigated is two connected integrate-and-fire networks, and that the effects found apply to that system and leave open the possibility that communication through coherence, in the strong, information transmission, sense analysed here, may be found in other model networks and in the brain. However, the model described here is rather prototypical of connected cortical networks (Rolls, 2008b).

It was possible that different effects would be found if for example the communication is to a network that does not enter a categorical, decision-related state. In this case, the information transmission was measured by the mutual information between the stimulus s applied to the first network and the firing rates r in the second network. We found that in that case the information transmission was still high at low values of the forward coupling ω_f between the two networks that were insufficient to produce phase-locking, and that the information transmission and the response times were not affected by the phases of gamma oscillations induced in the two networks Net 1 and Net 2 (Figs 10 and 11).

We emphasize that the model described here is representative of the operation of the cerebral cortex in a number of ways. First, Net 1 showed a considerable change in its firing rate when it responded to its input, as illustrated in Fig. 2 in which the spontaneous rate of a single neuron was 3 spikes/s and the firing rate of the same neuron when N1 was responding to the inputs it received was ~ 40 spikes/s. Such large changes in firing rate are found in many cortical areas when neurons respond in the awake behaving monkey to effective stimuli (Rolls & Treves, 2011). For example, when neurons in the inferior temporal

FIG. 7. Decision time with phase control. (B) The mean decision time (ms; across 1000 trials) as a function of the relative phases of Net 1 D1 to Net 2 D2 produced by 60-Hz modulatory sine waves applied to the external inputs influencing the neurons in Net 1 pool 1 (N1D1) and Net 2 pool 1 (N2D1) through $\lambda_f = 0.015$. (A) Phase at different frequencies as a function of time in the trial showing that, after the decision cues and the external sine waves are applied with a phase of 180° starting at 1000 ms, the relative phases of the firing rates of N1D1 and N2D2 are well separated. (C) Phase at different frequencies as a function of time in the trial, showing that after the decision cues and the external sine waves are applied with a phase of 0° starting simultaneously at 1000 ms, the relative phases of the firing rates on N1D1 and N2D2 are close to 0° apart. Phase control of the firing of N1D1 and N2D2 did not affect the decision times.

visual cortex respond with sparse distributed tuning to objects or faces, the firing rates of single neurons to the most effective stimuli suddenly increase with latencies of typically 90–100 ms to 50–100 spikes/s (Rolls & Tovee, 1995; Tovee & Rolls, 1995; Rolls *et al.*, 1997a,b; Booth & Rolls, 1998; Rolls *et al.*, 2003b; Rolls *et al.*, 2004; Rolls & Treves, 2011; Aggelopoulos *et al.*, 2005; Aggelopoulos & Rolls, 2005). This happens for example when a saccade occurs to fixate an effective stimulus in a complex natural scene (Rolls *et al.*, 2003a). In the primary taste cortex in the insula and adjoining frontal operculum, neurons typically increase from very low spontaneous rates to firing rates of 20 or more spikes/s when an effective taste or oral texture or temperature stimulus is delivered (Scott *et al.*, 1986; Yaxley *et al.*, 1990; Verhagen *et al.*, 2004; Kadohisa *et al.*, 2005). The same happens in the secondary taste cortex and other regions of the orbitofrontal cortex (Rolls *et al.*, 1989, 1990, 1996c, 1999, 2003c, 2010c; Verhagen *et al.*, 2003;

Kadohisa *et al.*, 2004), and in the tertiary taste cortex in the anterior cingulate cortex (Rolls, 2008a). The same happens in the secondary olfactory cortex in the orbitofrontal cortex (Critchley & Rolls, 1996a,b; Rolls *et al.*, 1996a,b). Neural responses in the same range are also found to familiar visual stimuli in the perirhinal cortex (Hölscher *et al.*, 2003), to head direction in the presubicular cortex (Robertson *et al.*, 1999), and to fixated visual stimuli in the parietal cortex area 7 (Rolls *et al.*, 1979). Thus large changes in firing rate of the type modelled in this investigation are found in many cortical areas, and this is the quantitatively important way in which information is encoded in the cerebral cortex (Rolls, 2008b; Rolls & Treves, 2011). Second, the cerebral cortex is characterised by short-range excitatory recurrent collaterals between nearby pyramidal cells, and by longer-range connections, typically to and from the next layer in a cortical hierarchy (Rolls, 2008b; Chapter 1). The short-range connections are modelled by

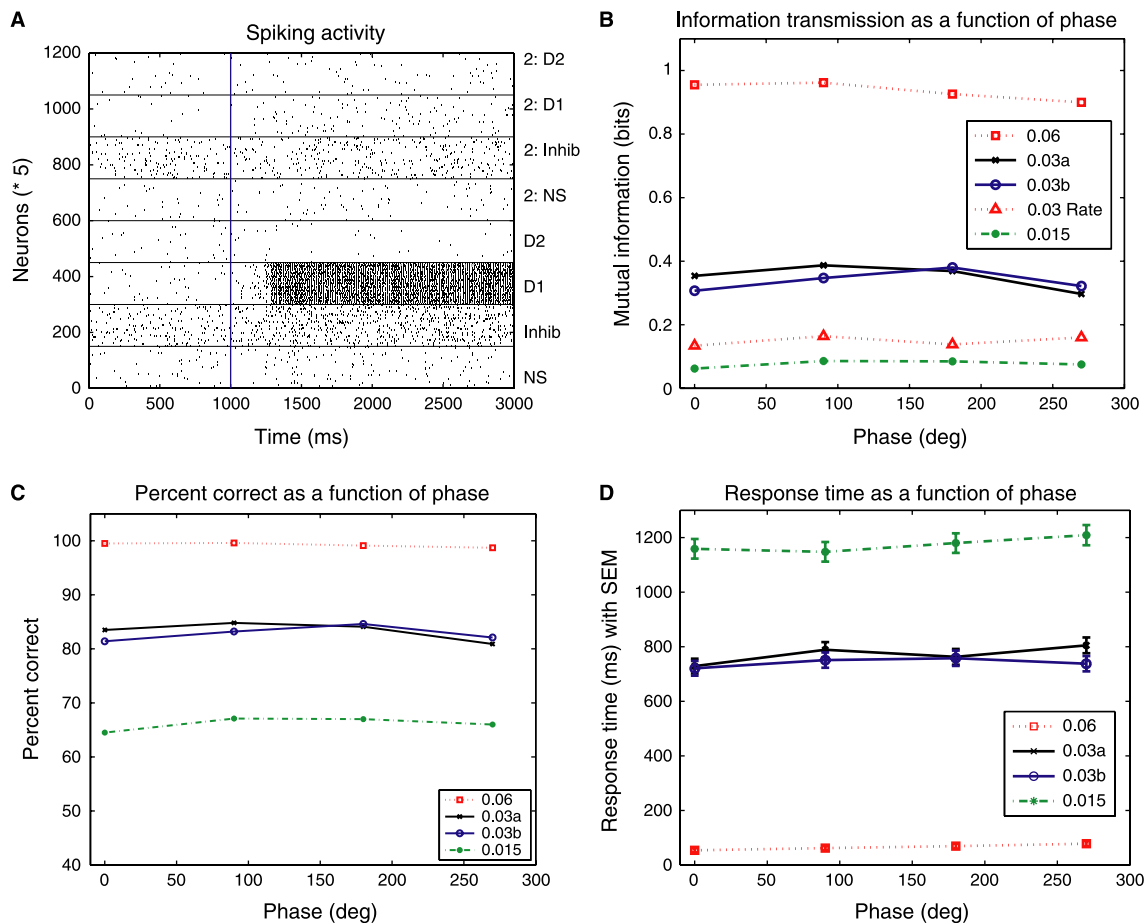


FIG. 10. Information transmission from Net 1 with gamma oscillations to Net 2 when Net 2 is operating without a high firing rate attractor state, as a function of the phase between the two networks controlled by external sine wave rate modulation at 60 Hz (which started at time 0). Results are shown for values of the forward coupling weight ω_f 0.015, 0.03 (two separate runs of 1000 trials each labelled 0.03a and 0.03b), and 0.06. (A) Rastergram of a typical trial with phase = 0. (B) Information transmission for different simulation runs of 1000 trials each. The information was measured by the decoding method from the firing rates for these plots using Eqn 15, and from the firing rates directly using Eqn 16 where labelled '0.03 Rate' (see Materials and methods). (C) Percentage correct (i.e. which Net 2 pool showed a significant increase in its firing rate after N1D1 increased its firing rate). (D) Response time \pm SE calculated over 800 trials for a significant increase in firing in N2D1 relative to N2D2.

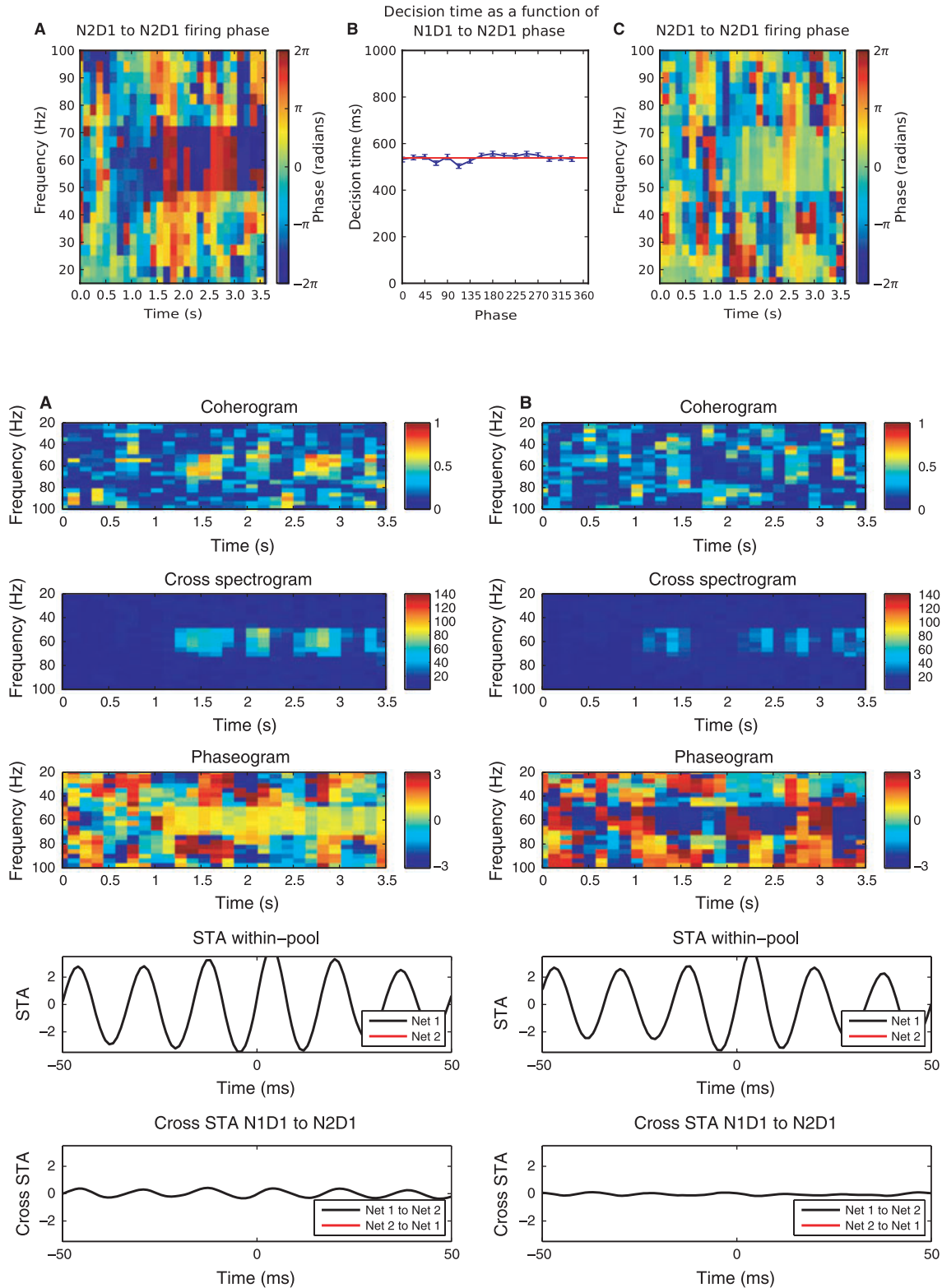


FIG. 11. Spectral analyses as a function of time for a single trial for the phase control investigation when Net 2 is operating without a high firing rate attractor state. These spectral analyses are for the data shown in Fig. 10. (A) Gamma phase control at 60 Hz applied to N1D1 and N2D1 with a phase lag of 0° . (B) Gamma phase control at 60 Hz applied to N1D1 and N2D1 with a phase lag of 180° . The results shown are for the AMPA case with $\omega_f = 0.06$. Top: coherogram between the LFPs in Net 1 D1 and Net 2 D1. Plot 2: cross spectrogram between the LFPs in Net 1 D1 and Net 2 D1. Plot 3: phaseogram between the firing rates in Net 1 D1 and Net 2 D1. Plot 4 black: the spike-triggered average (STA) between the spikes in Net 1 D1 and the LFPs in Net 1 D1; red: the STA between the spikes in Net 2 D1 and the LFPs in Net 2 D1 (there were too few spikes in Net 2 for a meaningful plot). Plot 5 black: the cross spike-triggered average (cross STA) between the spikes in Net 1 D1 and the LFPs in Net 2 D1; red: the cross STA between the spikes in Net 2 D1 and the LFPs in Net 1 D1 (there were too few spikes in Net 2 for a meaningful plot). The STA and crossSTA are for the 512 ms time period starting at $t = 2000$ in the trial, i.e. 1000 ms after the cues have been applied to N1 D1, with it entering an attractor state at approximately 500 ms later, at $t = 1300$ ms into the trial.

the recurrent collaterals within a network and the longer-range connections by the connections between Nets 1 and 2. Third, the connections in the backward direction end on the apical dendrites of cortical pyramidal cells in layer 1, and are therefore likely to be weaker than and shunted by the forward connections onto a pyramidal cell, which synapses onto the parts of dendrites closer to the cell body (Rolls, 2008b; Section 1.11, pp. 31–36). That is also part of what we modelled. Fourth, the connections between cortical areas must be sufficiently weak that connected cortical networks can have separate attractor states, otherwise the memory capacity of the whole of the cerebral cortex would be set by the number of recurrent collateral connections onto any one neuron in any one cortical area (O’Kane & Treves, 1992; Rolls, 2008b; Chapter 1). That also is part of what we modelled, by having weaker excitatory connections between the two connected networks than within each of the networks. Fifth, we not only modelled the situation in which the second network entered a decision attractor state, as happens in decision-making and memory recall parts of the cortex (Rolls & Deco, 2010; Deco *et al.*, 2012; see also Figs 2–9), but also the situation in which the second network does not enter an attractor state but is still influenced by the inputs from the first network (Figs 10 and 11). Sixth, we modelled a dynamically plausible system with integrate-and-fire neurons and dynamically modelled synapses that allowed the generation of gamma oscillations by reducing the $g_{\text{NMDA}}/g_{\text{AMPA}}$ synaptic conductance ratio. Thus the model described here is representative of the operation of the cerebral cortex in a number of key ways. Further, attractor models have been applied to many aspects of cortical function (Wang, 2008; Rolls & Deco, 2010; Deco *et al.*, 2012), and the model described here is a generic attractor model.

The following points show that the integrate-and-fire model used in the present research is appropriate for modelling the effects of gamma-band activity during cortical communication.

First, the model we have described and with which we obtained the findings here is not only generically, as just described, an appropriate model that captures important properties of cortical architecture, but also has been applied to and accounts for much experimental data on cortical neuronal activity, and in this sense too is an appropriate model for analysing communication between cortical networks. For example, this integrate-and-fire model accounts for the activity of prefrontal cortex neurons during the switching of attentional tasks in which there is a delay (Deco & Rolls, 2003). The same integrate-and-fire model can account for the responses of neurons in V2 and V4 during top-down attentional bias (Deco & Rolls, 2005a). The same integrate-and-fire model can account for the responses of neurons in the ventral premotor cortex and related areas during sequential vibrotactile decision-making (Deco & Rolls, 2006; Deco *et al.*, 2010, 2012; Martinez-Garcia *et al.*, 2011). The same model makes predictions, confirmed in fMRI investigations, about neuronal and synaptic activity and thus fMRI BOLD signals in the medial prefrontal cortex area 10 during decision-making tasks (Rolls *et al.*, 2010a,b).

Second, because the integrate-and-fire model has AMPA, NMDA and GABA receptors, each with their different time constants, the effects of which are modelled by the dynamics of the synapses (Eqn 10), then gamma oscillations can be facilitated by reducing the ratio $g_{\text{NMDA}}/g_{\text{AMPA}}$ as described here and by Buehlmann & Deco (2010).

Third, we showed that the same effects were found, that communication occurred before gamma coherence was induced by increasing the synaptic coupling between the networks, both when the receiving network operated as an attractor decision-making network (Figs 2–9) and when it operated as a network without a decision state in which the firing rates of the neurons in Net 2 continuously varied with the firing rates in Net 1 (Figs 10 and 11).

Fourth, we showed that when the network was in a spontaneous firing-rate state, before stimuli were applied, then no gamma oscillations were present. The gamma only started in the networks when inputs produced high firing rates (in practice typically 20 spikes/s or higher). We were able to show this by the use of the multitaper time spectrograms (Fries *et al.*, 2008; Mazzone *et al.*, 2008) shown for example in Figs 4 and 11, which are important during neurophysiological investigations of cortical communication to examine exactly when gamma coherence may start in relation to the transmission of information. Indeed, that is one of the important points and predictions for neurophysiological investigations that arise from the present work – gamma oscillations and coherence with input networks are predicted not to be present in receiving networks when they are in the spontaneous firing-rate state, and may only arise after the receiving network had increased its firing rate as a result of the information transmission. In this situation the research described here makes the important point that information transmission can occur with synaptic connection strengths between networks and signal strengths in the first network that may not be sufficient to produce coherence between the networks. It will be important to test that prediction neurophysiologically, taking care with spectrograms and coherence analysis as a function of time to measure when coherence may start between the networks in relation to when the second network shows influences from the first network and thus information transmission. Indeed, at least part of what is predicted, and thereby the applicability of the model described here, is already known – neurophysiological investigations have shown that cortical networks in V4 have little gamma-band oscillation (30–70 Hz) in the spontaneous firing-rate state, and gamma oscillations only become pronounced when the neurons have been induced to increase their firing rates by an input stimulus (Fries *et al.*, 2008). It is exactly this issue that is at the heart of this paper – if coherence becomes present between cortical networks, does it just reflect information transmission that has already occurred and has produced high firing rates in two strongly coupled networks which then begin to oscillate? If coherence between neurons increases with for example attentional modulation (Fries *et al.*, 2008), is this effect distinct from effects of firing rates, with higher firing rates tending to be related to more coherence, as described here? However, we note that in the present work we have gone beyond previous neurophysiological investigations that described spike coherence within networks in V4 (Fries *et al.*, 2008) to a situation in which information communication between different networks is being investigated, in the present investigation from Net 1 to Net 2.

We note that correlative evidence suggesting communication through coherence (Fries, 2005, 2009), such as the finding that gamma-band synchronization predicts speed of change detection (Womelsdorf *et al.*, 2006) and selective attention (Fries *et al.*, 2008), must be carefully evaluated in the light of the present findings. For example, gamma synchronization tends to become high when the coupling between networks is increased to high values (Fig. 5). This could be produced by any change such as increased attention or arousal on some trials which influenced synaptic transmission, for example increasing synaptic transmission by the release of acetylcholine, which would effectively increase the synaptic coupling between networks by reducing synaptic adaptation (Rolls, 2008b). However, in addition, a change that was associated with increasing the synaptic coupling ω_f and ω_b in our simulations was that the firing rate was also increased (Fig. 6), and that alone is an important factor that can increase the speed of information processing and decrease decision times (Rolls, 2008b; Rolls *et al.*, 2010a,b; Rolls & Treves, 2011). For these reasons, care must be taken before concluding that synchronization affects even the speed of information transmission, as well as the information transmission, as the underlying causal factors including any differences in firing rates must be analyzed. In the

network described here, because the parameters were under full control we were able to test whether in this system coherence facilitates communication as measured by information transmission and the speed of processing, and found that information transmission, and fast processing, occur before coherence sets in when oscillations are present (the AMPA case), and can occur without oscillations or synchrony just as well (the NMDA case; see Fig. 5). Further, even on trials when phase synchronization was present, the synchronization was delayed to be often 100 ms or more later than the decision time. Running correlations between the gamma-filtered LFPs in Net 1 and Net 2 confirmed this. This makes an important point – it is important to measure the oscillations and synchrony just at the time that the information transmission is occurring, not some time after that, as oscillations, and synchrony if present, occurred only when the firing rates of the neurons were becoming high in the attractor state, when the transition had already occurred from the spontaneous firing rate state. In the light of the present studies, further neurophysiological studies are needed to test whether synchrony plays a causal role in information transmission and the speed of information processing.

The results described here are consistent with previous studies which showed that fast ongoing fluctuation effects in model and real neural systems can be reflected in measures such as the power correlation, the spike-triggered average and the transfer entropy, of the neuronal (including multiple unit) activity, and the LFPs (Fries, 2005, 2009; Womelsdorf *et al.*, 2007; Buehlmann & Deco, 2010). What is new about the present investigation is that we measured how information transmission about an external stimulus from one network to a second network, i.e. information about which stimulus has been presented, is influenced by gamma oscillations and synchrony. We found in the system analysed that, at values of the coupling strength between the two networks that were sufficient for information transmission in this strong sense relevant to brain function, coherence was not present and phase did not affect the speed of information transmission, even though gamma oscillations were present. Thus communication in this strong sense of information transmission about an external event did not need coherence, and was not affected by the phase if coherence was present. The results were found for a simple and clearly defined model of coupled cortical attractor networks, and do not necessarily apply to all systems of coupled networks. Communication through coherence may be found in other scenarios.

The findings suggest that experimental investigations of whether information transmission in this strong sense is influenced by the coherence of oscillations, if oscillations are present, may be important for analysing the role of oscillations in information processing in the brain. The finding that gamma oscillations are not present during spontaneous firing, and only start in Net 2 when the neurons increase their firing rates, is illustrated by the single-trial type of analysis shown in Fig. 4. However, when the Net 2 D1 neurons selectively increase their firing rates the decision has effectively been taken, that is, the bifurcation has been crossed. This is one of the implications of the investigations described here – great care has to be taken using single-trial analyses with neurophysiological data to measure exactly when the gamma oscillations start, and also when any synchrony starts that may be present, in relation to the time of the decision or more generally of the information transmission.

Supporting Information

Additional supporting information may be found in the online version of this article:

Data S1. Supplementary material.

Please note: As a service to our authors and readers, this journal provides supporting information supplied by the authors. Such materials are peer-reviewed and may be re-organized for online delivery, but are not copy-edited or typeset by Wiley-Blackwell. Technical support issues arising from supporting information (other than missing files) should be addressed to the authors.

Acknowledgements

The research was supported by the Oxford Centre for Computational Neuroscience. G.D. received support from the McDonnell Centre for Cognitive Neuroscience at Oxford University, and from grant CONSOLIDER Bilingualism and Cognitive Neuroscience and project BFU (Spanish Ministry of Science). The authors declare no conflict of interest.

Abbreviations

AMPA_{ext}, AMPA from external connections; AMPA_{rec}, AMPA from recurrent collateral connections; cross-STA, cross spike-triggered average; CSM, cross-spectral density magnitude; D1, decision neuronal population 1 (decision pool 1); D2, decision pool 2; LFP, local field potential; N1D1, Network 1 decision pool 1; N2D1, Network 2 decision pool 1; N_E , number of excitatory neurons; N_{Ef} , number of neurons in a decision pool; Net 1, Network 1; Net 2, Network 2; N_I , number of inhibitory neurons; PSD, power spectral density; STA, spike-triggered average; δ , g_{AMPA}/g_{NMDA} modification ratio.

References

- Aggelopoulos, N.C. & Rolls, E.T. (2005) Natural scene perception: inferior temporal cortex neurons encode the positions of different objects in the scene. *Eur. J. Neurosci.*, **22**, 2903–2916.
- Aggelopoulos, N.C., Franco, L. & Rolls, E.T. (2005) Object perception in natural scenes: encoding by inferior temporal cortex simultaneously recorded neurons. *J. Neurophysiol.*, **93**, 1342–1357.
- Albantakis, L. & Deco, G. (2009) The encoding of alternatives in multiple-choice decision making. *Proc. Natl. Acad. Sci. U.S.A.*, **106**, 10308–10313.
- Bendat, J.S. & Piersol, A.G. (Eds) (2010) *Random Data: Analysis and Measurement Procedures*, 4th Edn. Wiley, New York, NY.
- Booth, M.C.A. & Rolls, E.T. (1998) View-invariant representations of familiar objects by neurons in the inferior temporal visual cortex. *Cereb. Cortex*, **8**, 510–523.
- Brunel, N. & Wang, X.J. (2001) Effects of neuromodulation in a cortical network model of object working memory dominated by recurrent inhibition. *J. Comput. Neurosci.*, **11**, 63–85.
- Brunel, N. & Wang, X.J. (2003) What determines the frequency of fast network oscillations with irregular neural discharges? I. Synaptic dynamics and excitation-inhibition balance. *J. Neurophysiol.*, **90**, 415–430.
- Buehlmann, A. & Deco, G. (2008) The neuronal basis of attention: rate versus synchronization modulation. *J. Neurosci.*, **28**, 7679–7686.
- Buehlmann, A. & Deco, G. (2010) Optimal information transfer in the cortex through synchronization. *PLoS Comput. Biol.*, **6**, e1000934.
- Burkitt, A.N. (2006) A review of the integrate-and-fire neuron model: I. Homogeneous synaptic input. *Biol. Cybern.*, **95**, 1–19.
- Cover, T.M. & Thomas, J.A. (1991) *Elements of Information Theory*. Wiley, New York, NY.
- Critchley, H.D. & Rolls, E.T. (1996a) Hunger and satiety modify the responses of olfactory and visual neurons in the primate orbitofrontal cortex. *J. Neurophysiol.*, **75**, 1673–1686.
- Critchley, H.D. & Rolls, E.T. (1996b) Olfactory neuronal responses in the primate orbitofrontal cortex: analysis in an olfactory discrimination task. *J. Neurophysiol.*, **75**, 1659–1672.
- Deco, G. & Rolls, E.T. (2003) Attention and working memory: a dynamical model of neuronal activity in the prefrontal cortex. *Eur. J. Neurosci.*, **18**, 2374–2390.
- Deco, G. & Rolls, E.T. (2005a) Neurodynamics of biased competition and cooperation for attention: a model with spiking neurons. *J. Neurophysiol.*, **94**, 295–313.
- Deco, G. & Rolls, E.T. (2005b) Synaptic and spiking dynamics underlying reward reversal in the orbitofrontal cortex. *Cereb. Cortex*, **15**, 15–30.

- Deco, G. & Rolls, E.T. (2006) A neurophysiological model of decision-making and Weber's law. *Eur. J. Neurosci.*, **24**, 901–916.
- Deco, G., Rolls, E.T. & Romo, R. (2010) Synaptic dynamics and decision-making. *Proc. Nat. Acad. Sci.*, **107**, 7545–7549.
- Deco, G., Rolls, E.T., Albantakis, L. & Romo, R. (2012) Brain mechanisms for perceptual and reward-related decision-making. *Prog. Neurobiol.*, [Epub 2 February.]
- Ding, M., Chen, Y. & Bressler, S.L. (2006) Granger causality: basic theory and application to neuroscience. In Schelter, B., Winterhalder, M. & Timmer, J. (Eds), *Handbook of Time Series Analysis*, chapter 17. Wiley, Weinheim, pp. 437–460.
- Fries, P. (2005) A mechanism for cognitive dynamics: neuronal communication through neuronal coherence. *Trends Cogn. Sci.*, **9**, 474–480.
- Fries, P. (2009) Neuronal gamma-band synchronization as a fundamental process in cortical computation. *Annu. Rev. Neurosci.*, **32**, 209–224.
- Fries, P., Reynolds, J., Rorie, A. & Desimone, R. (2001) Modulation of oscillatory neuronal synchronization by selective visual attention. *Science*, **291**, 1560–1563.
- Fries, P., Womelsdorf, T., Oostenveld, R. & Desimone, R. (2008) The effects of visual stimulation and selective visual attention on rhythmic neuronal synchronization in macaque area V4. *J. Neurosci.*, **28**, 4823–4835.
- Ge, T., Feng, J., Grabenhorst, F. & Rolls, E.T. (2012) Componential Granger causality, and its application to identifying the source and mechanisms of the top-down biased activation that controls attention to affective vs sensory processing. *Neuroimage*, **59**, 1846–1858.
- Granger, C.W.J. (1969) Investigating causal relations by econometric models and cross-spectral methods. *Econometrica*, **37**, 414–438.
- Gray, C.M., König, P., Engel, A.K. & Singer, W. (1989) Oscillatory responses in cat visual cortex exhibit inter-columnar synchronization which reflects global stimulus properties. *Nature*, **338**, 334–337.
- Gregoriou, G., Gotts, S., Zhou, H. & Desimone, R. (2009) High-frequency, long-range coupling between prefrontal and visual cortex during attention. *Science*, **324**, 1207–1210.
- Hölscher, C., Rolls, E.T. & Xiang, J.Z. (2003) Perirhinal cortex neuronal activity related to long term familiarity memory in the macaque. *Eur. J. Neurosci.*, **18**, 2037–2046.
- Ishiguro, K., Otsu, N., Lungarella, M. & Kuniyoshi, Y. (2008) Comparison of nonlinear granger causality extensions for low-dimensional systems. *Phys. Rev. E Stat. Nonlin. Soft Matter Phys.*, **77**, 036217.
- Kadohisa, M., Rolls, E.T. & Verhagen, J.V. (2004) Orbitofrontal cortex neuronal representation of temperature and capsaicin in the mouth. *Neuroscience*, **127**, 207–221.
- Kadohisa, M., Rolls, E.T. & Verhagen, J.V. (2005) Neuronal representations of stimuli in the mouth: the primate insular taste cortex, orbitofrontal cortex, and amygdala. *Chem. Senses*, **30**, 401–419.
- Knight, B. (2000) Dynamics of encoding in neuron populations: some general mathematical features. *Neural Comput.*, **12**, 473–518.
- Loh, M., Rolls, E.T. & Deco, G. (2007) A dynamical systems hypothesis of schizophrenia. *PLoS Comput. Biol.*, **3**, e228. doi:10.1371/journal.pcbi.0030228.
- Lungarella, M., Ishiguro, K., Kuniyoshi, Y. & Otsu, N. (2007) Methods for quantifying the causal structure of bivariate time series. *Int. J. Bifurcat. Chaos*, **17**, 903–921.
- Martinez-Garcia, M., Rolls, E.T., Deco, G. & Romo, R. (2011) Neural and computational mechanisms of postponed decisions. *Proc. Nat. Acad. Sci.*, **108**, 11626–11631.
- Mazzoni, A., Panzeri, S., Logothetis, N.K. & Brunel, N. (2008) Encoding of naturalistic stimuli by local field potential spectra in networks of excitatory and inhibitory neurons. *PLoS Comput. Biol.*, **4**, e1000239.
- Nordlie, E., Gewaltig, M.O. & Plesser, H.E. (2009) Towards reproducible descriptions of neuronal network models. *PLoS Comput. Biol.*, **5**, e1000456.
- O'Kane, D. & Treves, A. (1992) Why the simplest notion of neocortex as an autoassociative memory would not work. *Network*, **3**, 379–384.
- Panzeri, S. & Treves, A. (1996) Analytical estimates of limited sampling biases in different information measures. *Network*, **7**, 87–107.
- Renart, A., Parga, N. & Rolls, E.T. (1999a) Associative memory properties of multiple cortical modules. *Network*, **10**, 237–255.
- Renart, A., Parga, N. & Rolls, E.T. (1999b) Backprojections in the cerebral cortex: implications for memory storage. *Neural Comput.*, **11**, 1349–1388.
- Robertson, R.G., Rolls, E.T., Georges-François, P. & Panzeri, S. (1999) Head direction cells in the primate pre-subiculum. *Hippocampus*, **9**, 206–219.
- Rolls, E.T. (2008a) Functions of the orbitofrontal and pregenual cingulate cortex in taste, olfaction, appetite and emotion. *Acta Physiol. Hung.*, **95**, 131–164.
- Rolls, E.T. (2008b) *Memory, Attention, and Decision-Making. A Unifying Computational Neuroscience Approach*. Oxford University Press, Oxford.
- Rolls, E.T. & Deco, G. (2010) *The Noisy Brain: Stochastic Dynamics as a Principle of Brain Function*. Oxford University Press, Oxford.
- Rolls, E.T. & Tovee, M.J. (1995) Sparseness of the neuronal representation of stimuli in the primate temporal visual cortex. *J. Neurophysiol.*, **73**, 713–726.
- Rolls, E.T. & Treves, A. (1998) *Neural Networks and Brain Function*. Oxford University Press, Oxford.
- Rolls, E.T. & Treves, A. (2011) The neuronal encoding of information in the brain. *Prog. Neurobiol.*, **95**, 448–490.
- Rolls, E.T., Perrett, D., Thorpe, S.J., Puerto, A., Roper-Hall, A. & Maddison, S. (1979) Responses of neurons in area 7 of the parietal cortex to objects of different significance. *Brain Res.*, **169**, 194–198.
- Rolls, E.T., Sienkiewicz, Z.J. & Yaxley, S. (1989) Hunger modulates the responses to gustatory stimuli of single neurons in the caudolateral orbitofrontal cortex of the macaque monkey. *Eur. J. Neurosci.*, **1**, 53–60.
- Rolls, E.T., Yaxley, S. & Sienkiewicz, Z.J. (1990) Gustatory responses of single neurons in the orbitofrontal cortex of the macaque monkey. *J. Neurophysiol.*, **64**, 1055–1066.
- Rolls, E.T., Critchley, H.D., Mason, R. & Wakeman, E.A. (1996a) Orbitofrontal cortex neurons: role in olfactory and visual association learning. *J. Neurophysiol.*, **75**, 1970–1981.
- Rolls, E.T., Critchley, H.D. & Treves, A. (1996b) The representation of olfactory information in the primate orbitofrontal cortex. *J. Neurophysiol.*, **75**, 1982–1996.
- Rolls, E.T., Critchley, H., Wakeman, E.A. & Mason, R. (1996c) Responses of neurons in the primate taste cortex to the glutamate ion and to inosine 5'-monophosphate. *Physiol. Behav.*, **59**, 991–1000.
- Rolls, E.T., Treves, A. & Tovee, M.J. (1997a) The representational capacity of the distributed encoding of information provided by populations of neurons in the primate temporal visual cortex. *Exp. Brain Res.*, **114**, 149–162.
- Rolls, E.T., Treves, A., Tovee, M. & Panzeri, S. (1997b) Information in the neuronal representation of individual stimuli in the primate temporal visual cortex. *J. Comput. Neurosci.*, **4**, 309–333.
- Rolls, E.T., Critchley, H.D., Browning, A.S., Hernadi, A. & Lenard, L. (1999) Responses to the sensory properties of fat of neurons in the primate orbitofrontal cortex. *J. Neurosci.*, **19**, 1532–1540.
- Rolls, E.T., Aggelopoulos, N.C. & Zheng, F. (2003a) The receptive fields of inferior temporal cortex neurons in natural scenes. *J. Neurosci.*, **23**, 339–348.
- Rolls, E.T., Franco, L., Aggelopoulos, N.C. & Reece, S. (2003b) An information theoretic approach to the contributions of the firing rates and the correlations between the firing of neurons. *J. Neurophysiol.*, **89**, 2810–2822.
- Rolls, E.T., Verhagen, J.V. & Kadohisa, M. (2003c) Representations of the texture of food in the primate orbitofrontal cortex: neurons responding to viscosity, grittiness, and capsaicin. *J. Neurophysiol.*, **90**, 3711–3724.
- Rolls, E.T., Aggelopoulos, N.C., Franco, L. & Treves, A. (2004) Information encoding in the inferior temporal visual cortex: contributions of the firing rates and the correlations between the firing of neurons. *Biol. Cybern.*, **90**, 19–32.
- Rolls, E.T., Loh, M. & Deco, G. (2008) An attractor hypothesis of obsessive-compulsive disorder. *Eur. J. Neurosci.*, **28**, 782–793.
- Rolls, E.T., Grabenhorst, F. & Deco, G. (2010a) Choice, difficulty, and confidence in the brain. *Neuroimage*, **53**, 694–706.
- Rolls, E.T., Grabenhorst, F. & Deco, G. (2010b) Decision-making, errors, and confidence in the brain. *J. Neurophysiol.*, **104**, 2359–2374.
- Rolls, E.T., Critchley, H., Verhagen, J.V. & Kadohisa, M. (2010c) The representation of information about taste and odor in the primate orbitofrontal cortex. *Chemosens. Percept.*, **3**, 16–33.
- Salinas, E. & Sejnowski, T.J. (2001) Correlated neuronal activity and the flow of neural information. *Nat. Rev. Neurosci.*, **2**, 539–550.
- Schreiber, T. (2000) Measuring information transfer. *Phys. Rev. Lett.*, **85**, 461–464.
- Scott, T.R., Yaxley, S., Sienkiewicz, Z.J. & Rolls, E.T. (1986) Gustatory responses in the frontal opercular cortex of the alert cynomolgus monkey. *J. Neurophysiol.*, **56**, 876–890.
- Smerieri, A., Rolls, E.T. & Feng, J. (2010) Decision time, slow inhibition, and theta rhythm. *J. Neurosci.*, **30**, 14173–14181.
- Tiesinga, P.H. & Sejnowski, T.J. (2009) Cortical enlightenment: are attentional gamma oscillations driven by ING or PING? *Neuron*, **63**, 727–732.

- Tiesinga, P.H. & Sejnowski, T.J. (2010) Mechanisms for phase shifting in cortical networks and their role in communication through coherence. *Front. Hum. Neurosci.*, **4**, 196.
- Tovee, M.J. & Rolls, E.T. (1995) Information encoding in short firing rate epochs by single neurons in the primate temporal visual cortex. *Visual Cognition*, **2**, 35–58.
- Traub, R.D., Jefferys, J.G. & Whittington, M.A. (1997) Simulation of gamma rhythms in networks of interneurons and pyramidal cells. *J. Comput. Neurosci.*, **4**, 141–150.
- Treves, A. & Panzeri, S. (1995) The upward bias in measures of information derived from limited data samples. *Neural Comput.*, **7**, 399–407.
- Varela, F., Lachaux, J., Rodriguez, E. & Martinerie, J. (2001) The brainweb: phase synchronization and large-scale integration. *Nat. Rev. Neurosci.*, **2**, 229–239.
- Verhagen, J.V., Rolls, E.T. & Kadohisa, M. (2003) Neurons in the primate orbitofrontal cortex respond to fat texture independently of viscosity. *J. Neurophysiol.*, **90**, 1514–1525.
- Verhagen, J.V., Kadohisa, M. & Rolls, E.T. (2004) The primate insular taste cortex: neuronal representations of the viscosity, fat texture, grittiness, and the taste of foods in the mouth. *J. Neurophysiol.*, **92**, 1685–1699.
- Wang, X.J. (2002) Probabilistic decision making by slow reverberation in cortical circuits. *Neuron*, **36**, 955–968.
- Wang, X.-J. (2008) Decision making in recurrent neuronal circuits. *Neuron*, **60**, 215–234.
- Wang, X.J. (2010) Neurophysiological and computational principles of cortical rhythms in cognition. *Physiol. Rev.*, **90**, 1195–1268.
- Womelsdorf, T., Fries, P., Mitra, P. & Desimone, R. (2006) Gamma-band synchronization in visual cortex predicts speed of change detection. *Nature*, **439**, 733–736.
- Womelsdorf, T., Schoffelen, J.M., Oostenveld, R., Singer, W., Desimone, R., Engel, A.K. & Fries, P. (2007) Modulation of neuronal interactions through neuronal synchronization. *Science*, **316**, 1609–1612.
- Yaxley, S., Rolls, E.T. & Sienkiewicz, Z.J. (1990) Gustatory responses of single neurons in the insula of the macaque monkey. *J. Neurophysiol.*, **63**, 689–700.